Qin et al. Journal of Nanobiotechnology (2025) 23:201
https://doi.org/10.1186/s12951-025-03250-z

Journal of Nanobiotechnology

RESEARCH

Open Access

Mesenchymal stem cell-derived extracellular vesicles alleviate autism by regulating microglial glucose metabolism reprogramming and neuroinflammation through PD-1/PD-L1 interaction

Qian Qin[1], Linlin Fan[1], Xin Zeng[1], Danyang Zheng[1], Han Wang[1], Mengyue Li[1], Yutong Jiang[1], Hui Wang[1], Hao Liu[1], Shengjun Liang[1], Lijie Wu[1*] and Shuang Liang[1*]

Abstract
Neuroinflammation triggered by microglia activation is hallmark of autism spectrum disorder (ASD), and this process includes crucial metabolic reprogramming from oxidative phosphorylation to glycolysis, which may cause neuron loss and functional impairment. The inhibitory immune checkpoint programmed cell death protein 1 (PD-1) on immune cells is an important target for tumor immunotherapy. However, the immunomodulatory effects of PD-1 in ASD remains to be elusive. Mesenchymal stem cell-derived extracellular vesicles (MSC-EVs) exhibit immunomodulatory capabilities in a range of neurological diseases. Our findings indicated the expression of PD-L1 on MSC-EVs, potentially facilitating signaling to PD-1-expressing microglia. Here, we showed how MSC-EVs activated of PD-L1/PD-1 axis and ameliorated glycolysis, neuroinflammation and autism-like behaviors. After first detecting elevated glycolysis and neuroinflammation in prefrontal cortex (PFC) tissue from the maternal immune activation (MIA) mice, we also demonstrated that PD-1 expression level was upregulated in microglia. Following given MSC-EVs carried PD-L1 into adult MIA offspring mice via intranasal administration, which bound with PD-1 on microglia and then the autism-like behaviors were alleviated as well. Further experiments verified that MSC-EVs could decreased the level of glycolysis and neuroinflammation by PD-1/ERK/HIF-1α pathway in the primary microglia in PFC of MIA offspring mice. Pharmacological blockade and genetic inhibition of PD-1 could weaken the effect of MSC-EVs and aggravate microglial dysfunction, glycolysis and autism-like behaviors in MIA offspring mice. Futhermore, PD-L1 deficient weakened the effect of MSC-EVs on neuroinflammation, glycolysis and autism-like behaviors in MIA offspring mice. Our research indicated the significant immunomodulatory capabilities of MSC-EVs, which play an important role in reprogramming microglial glucose metabolism and suppressing neuroinflammation in ASD. By activating the PD-L1/PD-1 axis and inhibiting the downstream ERK/HIF-1α pathway,

*Correspondence:
Lijie Wu
wulijiehyd@126.com
Shuang Liang
liangyouyou2004@163.com
Full list of author information is available at the end of the article

MSC-EVs were found to alleviate autism-like behaviors, which revealing a novel pathological mechanism and offering promising therapeutic insights into ASD.

Graphical Abstract

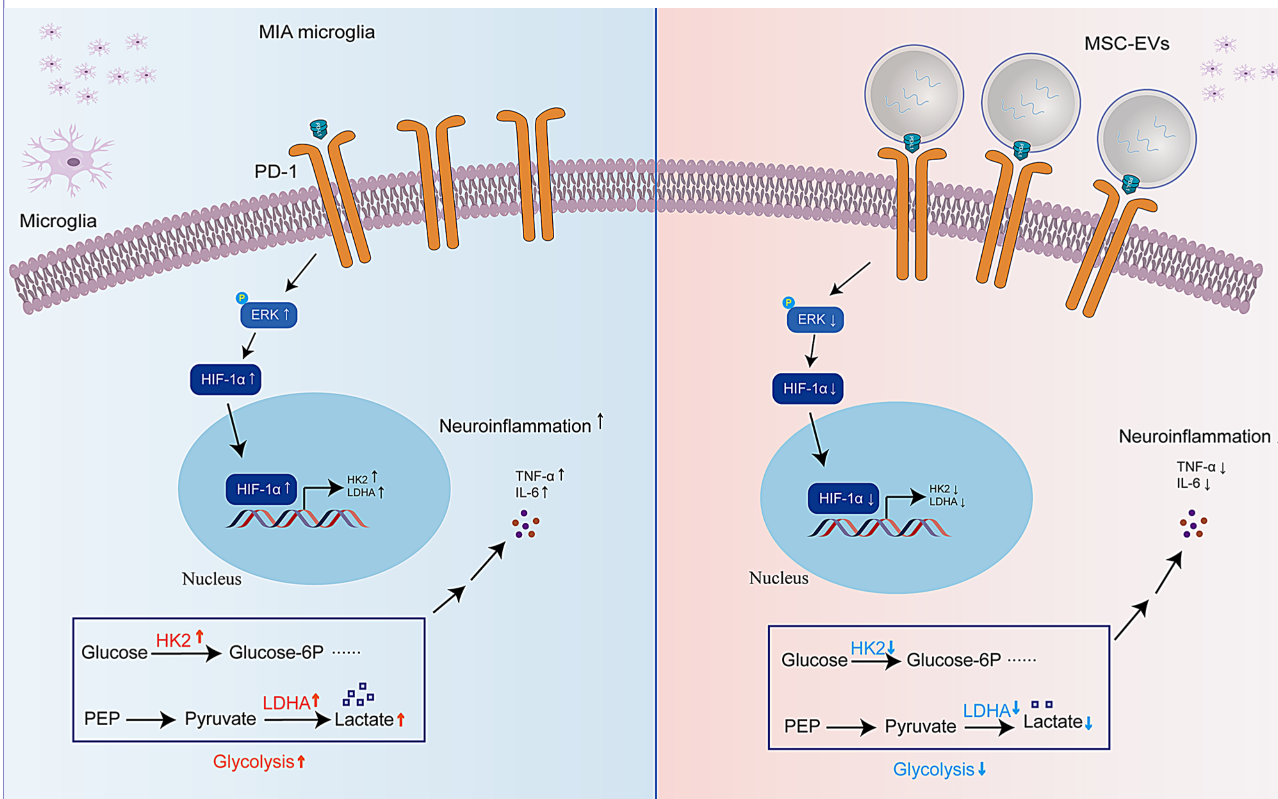

Keywords Autism spectrum disorder, MSC-EVs, PD-L1/PD-1, Glycolysis, Neuroinflammation

Introduction

Autism spectrum disorder (ASD) is currently one of the fastest-growing neurodevelopmental disorders characterized by high heritability and clinical heterogeneity, which leads to a huge socioeconomic burden [1]. Core symptoms of ASD include social impairments, repetitive behaviors and cognitive impairments. However, the underlying pathogenesis of ASD is still elusive.

Maternal immune activation (MIA) during pregnancy is a significant environmental risk factor to ASD [2]. As a viral mimic compound, Poly (I:C) was capable of mimicking the pathological process of virus-induced MIA, stimulating the production and releasing of pro-inflammatory factors. It is worth noting that these cytokines can cross the placental barrier, and then accumulate in the fetus, thereby damaging the fetal brain, transmitting long-term changes in neural development, further leading to occurrence of ASD in offsprings [2–4]. Clinical evidence suggested that ASD individuals across a wide age range exhibited significant neuroinflammation in the postmortem brain. Additionally, neuroinflammation is a well-recognized pathogenesis in ASD, characterized by prominent microglia activation and pro-inflammatory cytokines increasing in the brain and cerebral spinal fluid [5, 6].

The abnormally activated microglia plays a significant role in neuroinflammation, with potential for conversion from mitochondrial oxidative phosphorylation to glycolysis [7]. This metabolic shift triggers microglia to generate adenosine-triphosphate rapidly, and then enhancing its immune activation. Importantly, continuous glycolysis can produce lots of lactate which promotes plenty of pro-inflammatory cytokines release and accelerates microglial dysfunction in neurological diseases such as Alzheimer disease, ischemic stroke and multiple sclerosis [8]. Therefore, reprogramming microglial glucose metabolism could serve as a promising treatment strategy to alleviate neuroinflammation.

As an immune checkpoint hotspot, programmed cell death protein 1 (PD-1) is widely expressed on immune cells and a remarkable and high-efficient target in cancer immunotherapy. Upon binding with its ligand PD-L1, PD-1 can exert the immune inhibition capability [9]. Accumulating evidences have implicated that PD-1 was involved in multiple physiological and pathological processes within the central nervous system (CNS) [10]. Several studies have shown that PD-1 could express on the membrane of microglia, neuron and immune cells recruited from the periphery under physiological and pathological conditions [11], highlighting a crucial role of the PD-L1/PD-1 axis in maintaining immune homeostasis. PD-1 pathway can promote the production of IL-10 and suppress inflammatory response in improving Alzheimer's cognition [12]. In addition, PD-L1/PD-1 axis exhibits notable effect on the prevention of excessive neuroinflammatory response of traumatic brain injury [13].

Extracellular vesicles derived from mesenchymal stem cells (MSC-EVs) exhibit powerful immunomodulatory property and lower immunogenicity, which can cross the blood-brain barrier because of the nano size [14]. Interestingly, both MSCs and MSC-EVs highly express the immune checkpoint protein PD-L1. MSC could downregulate the activity of key enzyme HK2 by PD-L1/PD-1 axis, which further suppressed the glycolysis of T cell [15]. Li et al. [16] have found that the PD-L1 level was increased and then T cell activity was inhibited in patients after administrating the MSC-EVs in acute graft-versus-host disease Therefore, we aimed to elucidate the effect of MSC-EVs in immunomodulatory and glucose metabolic through PD-L1/PD-1 axis in ASD.

Here, we showed there was abnormally activated in microglia and glucose metabolism reprogramming in MIA-ASD model. After intranasal administration of MSC-EVs, we observed that PD-L1 was increased in the brain, which could reduce microglia activation and glycolysis process, and then improved the autism-like behavior in MIA offspring mice. In addition, the neuroinflammation and microglia activation were also inhibited while blocking the glycolysis process by 2-DG. Moreover, both the in vivo and in vitro analysis highlighted the pivotal roles of MSC-EVs by regulating ERK/HIF-1α pathway in MIA-induced ASD mice. Taken together, our results elaborated the mechanism of immunomodulatory and glucose metabolism reprogramming underlying PD-L1/PD-1 axis, thereby providing new insight and strategy for precision treatment in ASD.

Methods

Cell culture

The MSC derived from human umbilical cord used in this study were obtained from Nanjing Drum Tower Hospital. MSC were cultured in DMEM medium added 10% FBS and 1% penicillin-streptomycin. Primary mice microglia were isolated from postnatal (P1 to P3) mice as described in previous studies [17]. The process involved digesting the separated membranes and blood vessels, followed by trypsin digestion of brain tissue for 5 min. The digested tissue was filtered through a 70 μm sieve, followed by centrifugation to collect the cells. The collected cells were then suspended in DMEM/F12 medium added FBS and penicillin-streptomycin. When the cells reached 90% confluence, microglia were harvested by shaking the flasks at 225 rpm for 5 h. The microglia were collected and seeded into 6-well plates.

MSC cells were infected with a control lentivirus (MSC-EVs-Ctrl) or shCd274 lentivirus (MSC-EVs-shCd274), and the EVs were extracted using differential ultracentrifugation method.

Cell treatment

To explore the effect of MSC-EVs on microglia, PBS or MSC-EVs were co-cultured with microglia of MIA offspring mice with a dose of 50 μg, and the following groups were performed: C57BL/6J + PBS, C57BL/6J + MSC-EVs, MIA + PBS and MIA + MSC-EVs. For PD-1 inhibition studies, microglia of MIA offspring mice received PD-1 Ab (RMP1-14, 1 ug/10^6 cells, HY-P99144, MedChemExpress) or control IgG for 24 h before MSC-EVs treatment. For the glycolysis inhibition studies, microglia were treated with 2-DG (5 mM, A07816, Innochem) for 24 h. To detected the effect of MSC-EVs on ERK activation, we applied the ERK activator honokiol (20 μM, HY-N0003, MedChemExpress) to the treatment with MSC-EVs. We also applied the ERK inhibitor SL327 (10 μM, HY-15437, MedChemExpress) to treat with MSC-EVs and PD-1 Ab.

To explore the effect of PD-L1 of MSC-EVs on microglia in vitro, PBS, MSC-EVs-Ctrl or MSC-EVs-shCd274 were co-cultured with MIA primary microglia with a dose of 50 μg for 48 h, and the following groups were performed: PBS, MSC-EVs-Ctrl, MSC-EVs-shCd274.

Extraction and identification of MSC-EVs

MSC-EVs were separated from the supernatant of MSC through a series of centrifugation steps.When MSC cells reached the 90% confluence, they were cultured in serum-free DMEM. After 48 h, the supernatants were collected to extract EVs. Initially, the supernatant was centrifuged at 300 × g for 10 min, 2000 × g for 10 min, 10,000 × g for 30 min and 10,000 × g for 60 min at 4℃, followed by ultracentrifugation at 100,000 × g for 60 min using a CP100NX ultracentrifuge (Hitachi, Japan). The resulting pellet was resuspended in PBS and ultracentrifuged at 100,000 × g for 60 min again. Finally, the pellet was resuspended using PBS for further analysis. The EVs were visualized and quantified using the Nanometer particle size meter (Zetasizer Nano ZS90, Malvern, UK). The transmission electron microscopy (TEM) (H-7650, Hitachi, Japan) was used to observe the morphology of the

EVs. Western blotting analysis was conducted to confirm the EVs markers CD9, TSG101 and CD63.

Staining of MSC-EVs
The extracellular vesicles (EVs) were stained and purified according to previously established protocols [17]. The EVs protein concentration was adjusted to 100 μg/ml and co-incubated with Dil (C1036, Beyotime, China) for 15 min. Any excess dye was removed by incubating with 10% FBS to eliminate EVs. Subsequently, MSC-EVs samples were diluted using PBS and subjected to ultracentrifugation at 100,000 × g for 1 h. The resulting pellet was resuspended in PBS for the subsequent experiments.

Uptake of MSC-EVs into the primary microglia
The microglia (2×10^4 cells) were seeded in 35 mm dishes. After 24 h, 50 μg of Dil-labeled MSC-EVs were administered to the cultured cells. Following the incubation at 37 °C with 5% CO_2. Following incubation, the cells underwent three washes with PBS to eliminate the excess EVs. Then, the cells were stained with DAPI (Beyotime, China). The images were captured with Laser scanning confocal microscopes LSM 780 (Carl Zeiss, Germany).

Animal
C57BL/6J mice were procured from the Beijing Vital River Laboratory Animal Technology Co., Ltd. The mice were randomly allocated into distinct groups and maintained in a controlled environment with a 12-hour light/dark cycle, with a humidity of 55% ± 5%, a temperature of 21 °C ± 1 °C and enough food and water.

MIA mouse modeling
Pregnant C57BL/6J mice were administered intraperitoneally (*i.p.*) at a dose of 20 mg/kg poly(I:C) (Sigma-Aldrich) on embryonic day 12.5 (E12.5) for experimental purposes. The control group mice received an equivalent volume of PBS without any active compounds, ensuring a comparable handling procedure. Indeed, the number of male ASD patients is significantly higher than that of females [18, 19]. Noteworthy, the similar gender differences in autism-like behaviors have been observed in the MIA offspring mice, as confirmed in previous studies [20, 21]. Male offspring mice exhibit more pronounced autism-like behaviors compared to female offspring mice. Therefore, we chose male offspring mice for this study. After observing substantial gender disparities in the ASD-related traits of pups resulting from poly(I:C)-MIA offspring mice, we elected to focus solely on male offspring in our subsequent experiments.

Animal treatment
To explore the effect of MSC-EVs on ASD, each mouse was administration intranasally with 100 μg of MSC-EVs or equal volume PBS every day for 7 days, and the following groups were performed: C57BL/6J + PBS, C57BL/6J + MSC-EVs, MIA + PBS and MIA + MSC-EVs.

PD-1 Ab (RMP1-14) or control IgG were injected into MIA offspring mice using brain stereotaxic apparatus. Then, MSC-EVs were delivered into brain via intranasal administration daily for 7 days. Next, behavioral tests and molecular experiment were performed to evaluate the impact of PD-1 Ab on MIA offspring mice.

In brief, the anesthesia process was initiated in an induction chamber with a mixture of isoflurane and oxygen, initially administering 5 L per minute for induction, followed by approximately 3 L per minute to maintain anesthesia. Fur was removed from the skull's surface using clippers, and the area was disinfected using iodophor.

Place the mouse securely on a stereotactic stand and make a midline incision to expose the bregma. A burr hole was drilled precisely above the PFC, coordinates: AP: 1.90 mm from Bregma, DV: ±0.30 mm, ML: 2.26 mm) using a high-precision Kopf micro-manipulator. PD-1 antibody (Ab) or IgG was administered slowly, at a rate of 60 nanoliters per minute, employing a pico-spritzer air puffer system. After the targeted volume of the reagent had been administered, the pipette was maintained in its position for a duration of 5 min before being gradually withdrawn from the brain. For glycolysis studies, male MIA offspring mice were intraperitoneal (*i.p.*) injection of 2-DG (250 mg/kg, A07816, Innochem) or PBS for 7 days.

The pAAV-Iba-1-eGFP-Pdcd1-shRNA (AAV-Iba-1-shPdcd1, serotype MG1.2) (GenePharma, Shanghai, China) was used to target Iba-1^+ cells and interrupt PD-1 expression in microglia, and pAAV-Iba-1-eGFP-MCS used as a control vector (AAV-Ctrl). Briefly, the MIA offspring mice were placed in a stereotaxic apparatus, and was injected the viral vector (5×10^9 vg; 500 nl) into the PFC (coordinates: AP:1.90 mm, DV:0.30 mm, ML:2.26 mm) by a 10 μl syringe (Hamilton) connecting to a micro-syringe pump controller at a speed of 60 nl/min. Three weeks later, MSC-EVs were delivered into brain by intranasal administration once a day for one week. Next, behavioral tests and molecular experiment were performed to evaluate the impact of AAV-shPdcd1 on MIA offspring mice.

To explore the effect of PD-L1 of MSC-EVs on neuroinflammation, glycolysis and autism-like behaviors in vivo, 100 μg MSC-EVs-shCd274, MSC-EVs-Ctrl or equal volume PBS was respectively administrated intranasally into MIA offspring mice daily for 7 days.

Behavioral experiments
All behavioral assessments were conducted in a quiet setting, with a consistent scorer. The mice have adapted to the testing room for a minimum of three hours prior

to the commencement of each behavioral examination to ensure minimal stress and accurate scoring. Animals completed the three-chamber test, Open field test (OFT), Elevated plus maze (EPM) test, Novel object recognition test (NOR), Grooming test and Marble burying test (MBT) as described in the Supplementary Information.

Cell viability

In order to evaluate the cytotoxicity of MSC-EVs to primary mice microglia, the cells were cultured in a 96-well plate (1×10^4 cells/well). After 6 h of culture, the cell survival level was analyzed using the CCK8 assay on a microplate reader acc ording to the instructions (HY-K0301, MedChemExpress).

qRT-PCR and other experiments

The qRT-PCR, Western blot analysis, immunofluorescence and enzyme-linked immunosorbent assay (ELISA) methodologies were detailed in Supplementary Information. The primers and antibodies use in this study were showed in the Supplementary Tables 1 and Table 2, respectively.

Lactate level measurement

Lactate level was measured in mice serum and microglia culture supernatants via the lactate testing kit (A019-2-1, Nanjing Jiancheng Bioengineering Institute) following the manufacturer's protocol.

Data collection and preprocessing

The public datasets include the single-cell sequencing data of postmortem PFC tissue from 10 ASD patients and 7 normal (PRJNA434002) [22], microarray dataset of PFC tissue mRNA from 6 MIA offspring mice and 6 control mice. (GSE77972) [23] and the microarray dataset of postmortem FC tissue from 16 ASD patients and 16 normal developing children's tissue (GSE28521) [24].

For the chip data downloaded from the GEO database, probe-to-gene mapping was performed using the annotation files provided by the corresponding detection platform for each dataset. If a probe matches multiple genes simultaneously, the probe is removed; if multiple probes match the same gene, the mean detection abundance of these probes is taken as the final expression value for that gene.

The raw mRNA-seq expression profile data underwent conversion to Fragments Per Kilobase of transcript per Million Mapped Reads (FPKM) values, a measure of gene expression intensity. The FPKM values were then subjected to a log2 transformation (by adding 1 to the expression value) for standardization, serving as the final gene expression measure.

The data source is publicly available from the Sequence Read Archive (SRA, accession number PRJNA434002), with the sample were characterized as male and originating from the PFC. For the single-cell sequencing raw data (PRJNA434002), Cell Ranger software was employed for preprocessing, including FASTQ file generation, read alignment, and Unique Molecular Identifier (UMI) quantification. Cell Ranger was executed using default parameters, and the ENSEMBL GRCh38 reference genome was utilized to ensure comprehensive capture of intronic reads from the nuclear-enriched pre-mRNA transcriptome. The Seurat package in R was employed to generate Seurat objects for each specific cell type, housing scRNA-seq gene expression matrices. Batch correction and sample integration were subsequently executed through the IntegrateData function. To ensure data quality, cells were filtered according to the gene expression, retaining only those with a count of 200 to 4000 genes and less than 20% mitochondrial gene content. Normalization and scaling of the remaining scRNA-seq data were performed using NormalizeData and ScaleData. Principal component analysis (PCA) was conducted using RunPCA, and a Uniform Manifold Approximation and Projection (UMAP) was employed to condense the top principal components. Manual annotation of known gene markers was assigned to cell types. The Idents and DimPlot tools facilitated the annotation and visualization of both general cell types and their subtypes within the dataset.

Scoring of the inflammation for microglia was performed using a scoring system based on the gene sets related to inflammation were obtained using the "HALLMARK INFLAMMATORY RESPONSE" of Molecular Signatures Database (MSIGDB) (https://www.gsea-msigdb.org/gsea/msigdb).

Functional enrichment analysis

Upload the differentially expressed genes to the DAVID software (https://david.ncifcrf.gov/summary.jsp) [25], select OFFICIAL_GENE_SYMBOL as the gene identifier, and set the species to Homo sapiens or Mus musculus. Then conduct KEGG pathway enrichment analysis. Using $P<0.05$ as a threshold to screen KEGG pathway entries related to ASD as the main gene functional enrichment process and signaling pathways associated with ASD, predicting the pathological mechanisms of ASD. Subsequently, we conducted Gene Set Enrichment Analysis (GSEA) analysis [26] related pathway enriched by KEGG using the cluster Profiler package.

Statistical analysis

The GraphPad Prism 8.0.2 software (https://www.graphpad.com) was used to conduct the statistical analyses. For pairwise comparisons between two groups, an unpaired Student's t-test was employed. To evaluate multiple groups, the one/two-way ANOVA test were used. All data were analysed as mean ± SD, and statistical significance was showed as $^{*}P<0.05$, $^{**}P<0.01$ and $^{***}P<0.001$. Detailed information on the study design, replication numbers, and statistical tests employed are showed in figure legends.

Results

Construction of MIA model in pregnant and MIA offspring mice

C57BL/6J mice were injected (*i.p.*) with 20 mg/kg of poly(I:C) at E12.5 to construct the MIA model in pregnant stage (Fig. 1A). Then, after 3 h of poly(I:C) injection, the level of IL-6 and TNF-α in the placenta, serum, spleen and mesenteric lymph nodes of MIA pregnant mice were all significantly elevated, whereas no differences were detected in IL-1β, IL-4 and IL-10 (Fig. 1B-E). In summary, these results showed that MIA pregnant mice experienced acute inflammatory response.

When the MIA offspring mice grew to 8 weeks, we performed multiple behavioral tests to estimate the autism-like behaviors of mice. In the three-chamber test, social behaviors of mice were evaluated. During the first phase, PBS offspring mice prefered interacting with the stranger mouse 1 (S1) but not the empty cage. In contrast, MIA offspring mice did not exhibit a significant difference in the duration of exploring the empty cage compared to S1, suggesting a compromised social ability. In the second phase, PBS offspring mice spent longer time investigating the new stranger mouse 2 (S2) than S1, while MIA offspring mice spent no difference in contact time within S1 and S2, pointing to an impaired social preference pattern (Fig. 1F). Then, the OFT and EPM were employed to assess anxiety-related behaviors in mice. In the OFT test, a significant reduction in entry times in center zone and time spent in center zone were observed in MIA offspring mice compared to the PBS group (Fig. 1G). During the EPM assessment, the MIA offspring mice demonstrated less entries in open arms and shorter time in open arms (Fig. 1H), longer time in closed arms, while less zone transition times (Figure S1). However, there were no significant difference in mean speed and total moving distance between the two groups in OFT and EPM (Figure S1). These results indicated that MIA offspring mice spent less time exploring the central area or open arms due to anxiety and fear in unfamiliar environment. And this phenomenon was not caused by their basic motor ability.

Then, we conducted an assessment of stereotyped behaviors through the MBT and grooming test. In the MBT, MIA offspring mice demonstrated a higher tendency, burying an average of approximately nine marbles, in contrast to the PBS group mice, who typically buried around four marbles (Fig. 1I). And the results of grooming test revealed that MIA offspring mice exhibited a significantly increased frequency and time of self-grooming compared to the PBS group (Fig. 1J). These results suggested that MIA offspring mice showed presence of repetitive stereotyped behaviors.

To evaluate cognitive and memory performance, we employed the NOR test. Under normal circumstance, mice were exhibited a natural inclination for exploration of novel items, which shown as increased interest in touching or sniffing unfamiliar objects within a space. In the NOR test, we observed that during the initial familiarization phase, both MIA and PBS offspring mice displayed similar exploration duration for two identical objects, labeled a and b. However, during the testing phase, PBS offspring mice demonstrated a significantly higher level of curiosity towards a new object, c, which had replaced object b, while no difference in sniffing time between a and c of MIA offspring mice group. This difference in exploration time suggested that MIA offspring mice exhibited impaired cognitive and memory function (Fig. 1K). In summary, MIA offspring mice showed decreased social ability, impaired social preference, higher anxiety level, presence of repetitive stereotyped behaviors, and decreased cognitive ability. Therefore, MIA offspring mice could serve as a reliable model for subsequent ASD research.

The MIA offspring mice showed increased neuroinflammation

Neuroinflammation is characterized by an inflammatory reaction in either the CNS or peripheral nervous system (PNS). When neural tissues are infected, injured, or subjected to other stimuli, immune cells and inflammatory factors gather in the affected area, leading to the occurrence of neuroinflammation. Firstly, we detected significantly elevated level of the inflammatory factors IL-6 and TNF-α in the PFC tissue in fetal brain, P0 (newborn), 4-week-old, 8-week-old and serum in 8-week-old MIA offspring mice (Fig. 2A-B), indicating significant neuroinflammatory response in MIA offspring mice and exist for a long time. Notably, the PFC plays a pivotal role in regulating behaviors, including social interaction, cognitive ability, decision-making and emotional regulation. Furthermore, impairments in the PFC have been closely linked to the onset and progression of ASD. Activated microglia stimulate immune response by secreting large amounts of cytokines and neurotoxic factors, thereby triggering neuroinflammatory response. The level of Iba-1 in the PFC tissue slices of MIA offspring mice was significantly higher than that in control mice (Fig. 2C). To investigate the correlation between neuroinflammation and ASD individuals, we performed bioinformatics analysis using the publicly available GSE28521 dataset from the GEO database. This dataset contains transcriptomic data related to the PFC of individuals with ASD. Gene set enrichment analysis (GSEA) results showed that the inflammatory response, IL-6 production, tumor

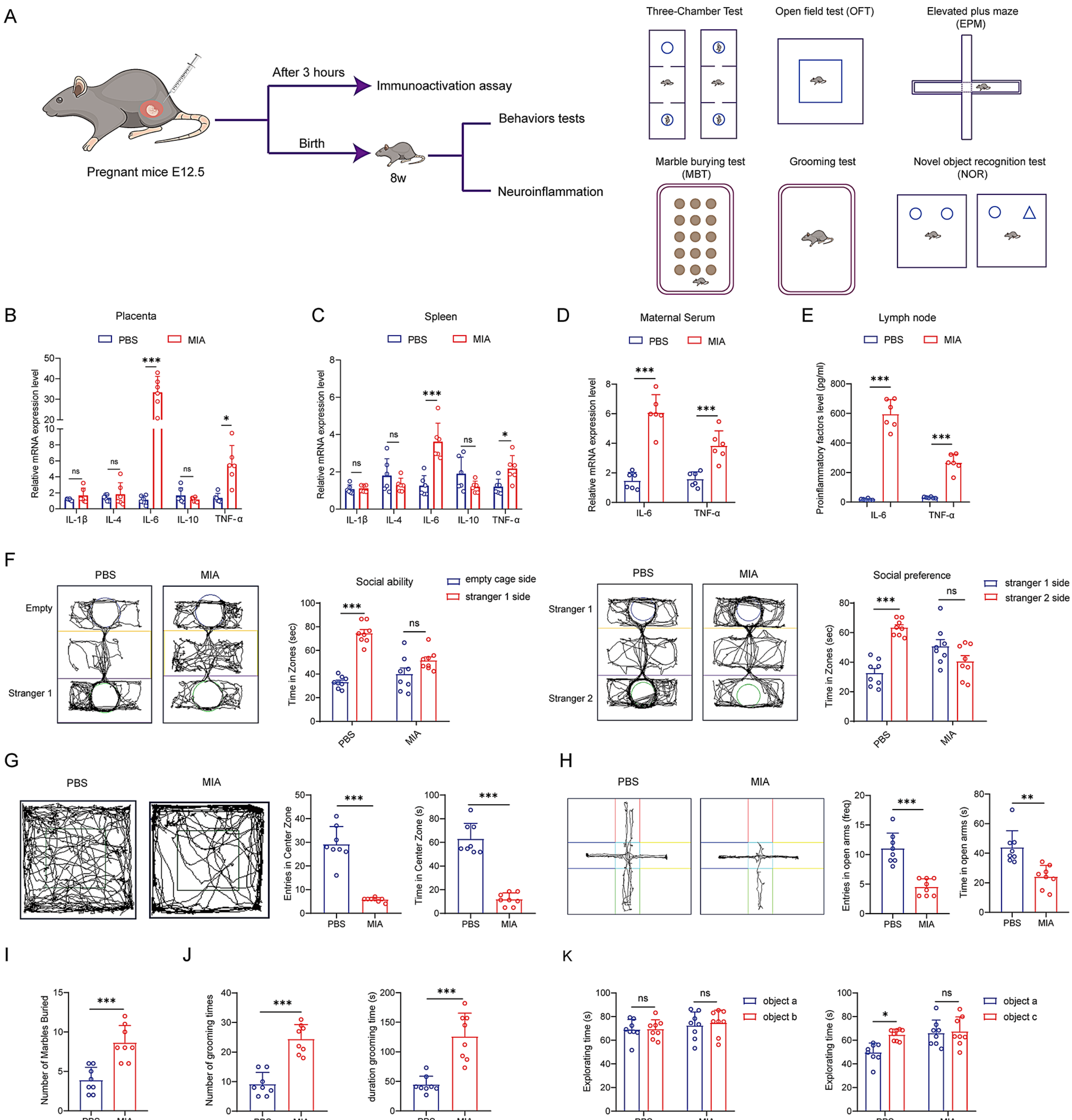

Fig. 1 MIA offspring mice showed typical autism-like phenotypes. (**A**) Schematic diagram illustrating the experimental procedure of MIA offspring mice. (**B**-**E**) The inflammatory factors detection in placenta, spleen, serum and lymph node by qPCR and ELISA between PBS and MIA maternal groups. *n*=6. Two-way ANOVA. (**F**) Trajectory route and statistical chart of sociability and social preference in the three-chamber test of PBS and MIA offspring mice. *n*=8. Two-way ANOVA. (**G**) Trajectory route and statistical chart of entries times in center zone and time in center zone in the OFT of PBS and MIA offspring mice. *n*=8. Student's *t*-test. (**H**) Trajectory route and statistical chart of entries in open arms and time in open arms in EPM test of PBS and MIA offspring mice. *n*=8. Student's *t*-test. (**I**) Statistical chart of number in marbles buried of PBS and MIA offspring mice. *n*=8. Student's *t*-test. (**J**) Statistical diagram of number of grooming times and duration grooming time of PBS and MIA offspring mice. *n*=8. Student's *t*-test. (**K**) Statistical diagram of exploration time for each object in the NOR test of MIA offspring mice. *n*=8. Two-way ANOVA. ns $P \geq 0.05$, *$P<0.05$, **$P<0.01$, ***$P<0.001$

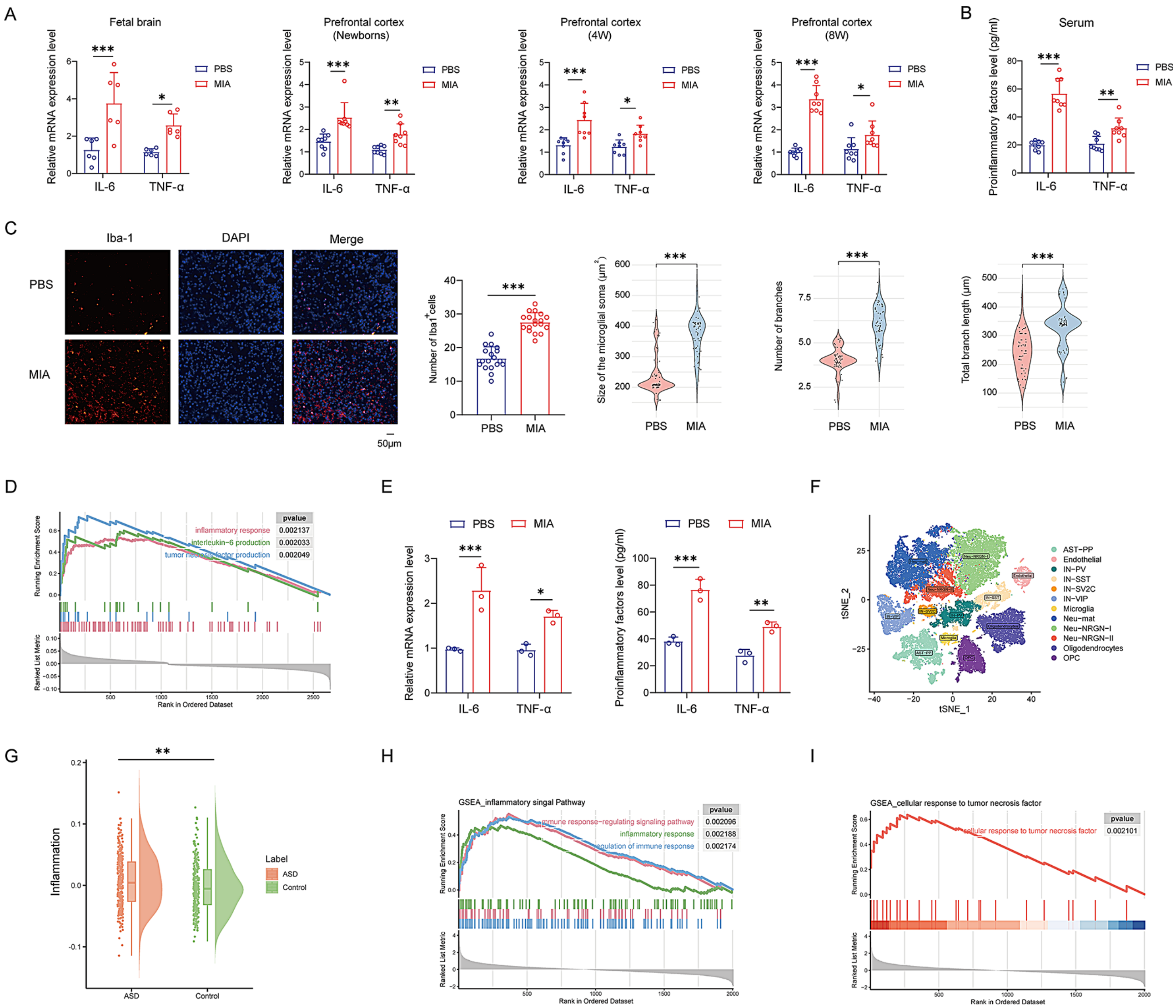

Fig. 2 The MIA offspring mice showed the activation of neuroinflammation and microglia. (**A**-**B**) IL-6 and TNF-α level detection of PFC and serum by qPCR and ELISA respectively between PBS and MIA offspring mice. *n*=6. Two-way ANOVA. (**C**) Immunostaining analysis of Iba-1$^+$ of PFC in PBS and MIA offspring mice. Scale bar = 50 μm. Student's *t*-test. (**D**) The results of GSEA enrichment in ASD and controls frontal cortex (GSE28521). (**E**) The IL-6 and TNF-α level assessment in microglia between PBS and MIA offspring mice. *n*=3. Two-way ANOVA. (**F**-**I**) Analysis of scRNA-seq dataset (PRJNA434002) in ASD patients and controls PFC: (**F**) tSNE visualization revealed 12 cell clusters; (**G**) Raincloud plot showed the inflammation score in microglia of ASD patients and controls; (**H**-**I**) GSEA enrichment analysis of 4 pathways according to the expressed profile in microglia cluster. ns $P \geq 0.05$, *$P<0.05$, **$P<0.01$, ***$P<0.001$

necrosis factor (TNF) production were up-regulated according to the expressed profile of GSE28521 dataset (Fig. 2D). In this study, we also observed that the level of IL-6 and TNF-α was increased in primary microglia from MIA offspring mice (Fig. 2E, Figure S2). Furthermore, we performed single-cell sequencing analysis of the public PRJNA434002 dataset, which includes 12 cell types. The rain-cloud plot illustrated that the inflammation score of microglia in the PFC of ASD patients was higher compared to that of controls (Fig. 2F-G). GSEA indicated that signaling pathways associated with the immune response, inflammatory response, regulation of immune response, and cellular response to tumor necrosis factor were activated in ASD patients, as evidenced by the gene expression profiles of microglia in the PRJNA434002 dataset (Fig. 2H-I).

MSC-EVs exhibit high expression of PD-L1, while MIA mouse brain tissue and microglia show high level of PD-1

The timelines and protocols were employed for isolation and characterization of MSC-EVs (Fig. 3A). NanoSight analysis results showed the size of MSC-EVs was ~180 nm in diameter (Fig. 3B). Furthermore, TEM demonstrated EVs with characteristic morphology enclosed by double membranesand exhibits a biconcave disk-like structure typical of EVs (Fig. 3C). Moreover, western

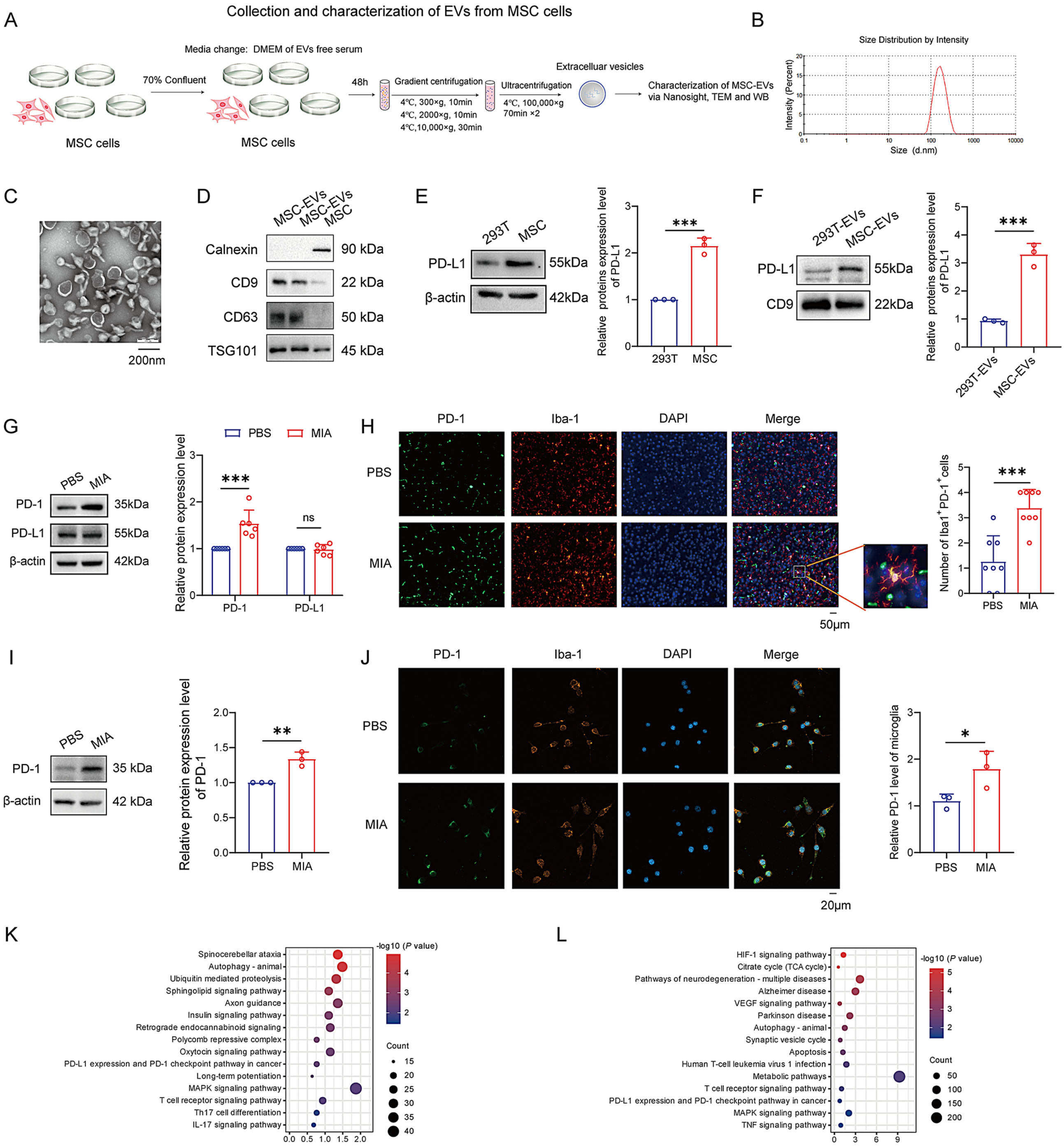

Fig. 3 High expression of PD-L1 in MSC-EVs, and high expression of PD-1 in MIA offspring mice. (**A**) Schematic diagram illustrating the extraction–separation process of MSC-EVs. (**B**-**D**) Characterization of MSC-EVs: (**B**) Size distribution of MSC-EVs measured using a nanoparticle size meter; (**C**) TEM of MSCs-EVs isolated from MSCs. Scale bar = 200 nm; (**D**) Western blot analysis of CD9, CD63, TSG101 and calnexin in MSC-EVs. (**E**-**F**) Western blot analysis of the expression of PD-L1 in MSCs and MSC-EVs. *n*=3. Student's *t*-test. (**G**) Western blot analysis of PD-1 and PD-L1 of PFC in PBS and MIA offspring mice. *n*=6. Two-way ANOVA. (**H**) Immunostaining analysis of co-localization of PD-1^+ and Iba-1^+ of PFC in MIA offspring mice. Scale bar = 50 μm. Student's *t*-test. (**I**) Western blot analysis of PD-1 in microglia in PBS and MIA offspring mice. *n*=3. Student's *t*-test. (**J**) Immunostaining analysis of co-localization of PD-1^+ and Iba-1^+ in microglia in PFC MIA offspring mice. Scale bar = 20 μm. Student's *t*-test. (**K**) KEGG analysis of the differentially expressed genes of PFC in MIA offspring mice and controls (GSE77972). (**L**) KEGG analysis of the differentially expressed genes of FC in ASD patients and controls (GSE28521).ns *P*≥0.05, **P*<0.05, ***P*<0.01, ****P*<0.001

blotting results showed the expression of the EVs-specific markers CD9, CD63 and TSG101 in the EVs formulation, but the cytoplasmic protein Calnexin was not expressed (Fig. 3D). The PD-L1 expression of surface of MSC and MSC-EVs were both significantly higher than the control group (Fig. 3E-F).

To further explore the effects of MSC-EVs on MIA offspring mice in vivo, we detected a significant increase in PD-1 level in the PFC of 8-week-old MIA offspring mice, while there was no significant difference in PD-L1 level between the two groups (Fig. 3G, Figure S3). Double immunofluorescence staining results showed that the expression level of PD-1 on the surface of microglia in the PFC of MIA offspring mice were significantly higher than those in the control group mice (Fig. 3H, Figure S4). Moreover, the expression level of PD-1 in primary microglia from MIA offspring mice was significantly upregulated (Fig. 3I-J). These results indicated that when MSC-EVs intervened, their surface PD-L1 could bind to PD-1 on the surface of activated microglia in the PFC of MIA offspring mice, thereby exerting immunomodulatory and anti-inflammatory effects.

In order to verify this, we conducted a biological functional analysis of ASD patients and MIA offspring mice using the public database. KEGG functional enrichment analysis based on the frontal cortex (FC) dataset GSE77972 of MIA offspring mice revealed that differential genes were significantly enriched in pathways such as PD-L1/PD-1 pathway (Fig. 3K). Additionally, KEGG functional enrichment analysis of differential genes in the PFC dataset GSE28521 of ASD patients showed potential abnormalities in pathways including PD-L1/PD-1 and TNF-α pathways (Fig. 3L). The collective evidence of substantial enrichment of the PD-L1/PD-1 pathway in both MIA offspring mice and patients with ASD also suggests a potential role for immune dysfunction in ASD, mediated through this axis.

The activation level of the ERK/HIF-1α pathway and Glycolysis were elevated in the MIA offspring mice

Increased glycolysis is a necessary condition for microglia activation and neuroinflammatory response. Compared to the control group, the expression level of HK2 and LDHA in the PFC tissue of MIA offspring mice as well as lactate level in the PFC and serum were elevated (Fig. 4A-C). And the expression level of HK2, LDHA and lactate level in the primary microglia of MIA offspring mice were all increased as well (Fig. 4I-J), indicating the glycolysis level was increased in the brain of MIA offspring mice.

Intervention with the glycolysis inhibitor 2-deoxyglucose-6-phosphate (2-DG) in MIA offspring mice for one-week resulted in decreased expression of HK2 and LDHA compared to the PBS group, along with a reduction in the production and secretion of IL-6 and TNF-α (Fig. 4D-H). Similar effects of 2-DG on glycolysis and inflammation were also observed in microglia from MIA offspring mice (Fig. 4K-O), suggesting that inhibiting glycolysis could reduce microglial activation.

Studies have shown that the activation of PD-L1/PD-1 axis could inhibit the phosphorylation of ERK in microglia [27]. And it has been demonstrated that HIF-1α is a key transcription factor for glycolysis-related genes, and upregulation of HIF-1α could promote an increase in glycolysis. Compared to control mice, the expression level of p-ERK//ERK and HIF-1α were upregulated, manifesting an elevated activation level of the ERK/HIF-1α pathway in the PFC and primary microglia of MIA offspring mice (Fig. 4P-S). These results suggested that the activation of the ERK/HIF-1α pathway in microglia of MIA offspring mice may promote intracellular glycolysis, which could be an important factor in microglia activation.

Moreover, the KEGG functional enrichment analysis of differential genes in the PFC dataset GSE28521 of ASD patients showed potential abnormalities in pathways including HIF-1α and TNF-α pathways (Fig. 3L). Additionally, gene set enrichment analysis (GSEA) of the ERK1 and ERK2 cascade, postive regulation of ERK1 and ERK2 cascade, regulation of ERK1 and ERK2 cascade and HIF-1 signaling pathway were all upregulated according to the expressed profile of GSE28521 dataset (Figure S5).

MSC-EVs could alleviate autism-like behaviors of MIA offspring mice

We administered 100 μg of MSC-EVs intranasally to each mouse daily for one week and conducted autism-related behavioral tests of mice after administration (Fig. 5A). Following the MSC-EVs intervention, the three-chamber test indicated an improvement in social ability and social preference in MIA offspring mice (Fig. 5B). In the OFT, the number of entries into the central zone and the time spent in the central zone were both increased in mice after MSC-EVs intervention (Fig. 5C, Figure S6). Results from the EPM test showed that following MSC-EVs intervention, MIA offspring mice exhibited increased activity distance, entries into the open arms and time spent in the open arms compared to the control group, while the time spent in the closed arms was significantly decreased (Fig. 5D, Figure S6). These results indicated that MSC-EVs intervention can improve anxiety level in MIA offspring mice. The MBT indicated a significant decrease in the number of marbles buried by mice after MSC-EVs intervention (Fig. 5E). The self-grooming test showed a significant decrease in both the frequency and duration of self-grooming in mice after MSC-EVs intervention, indicating an improvement in stereotyped behavior as well (Fig. 5F). In the NOR test, mice exhibited prolonged contact time with the novel object after

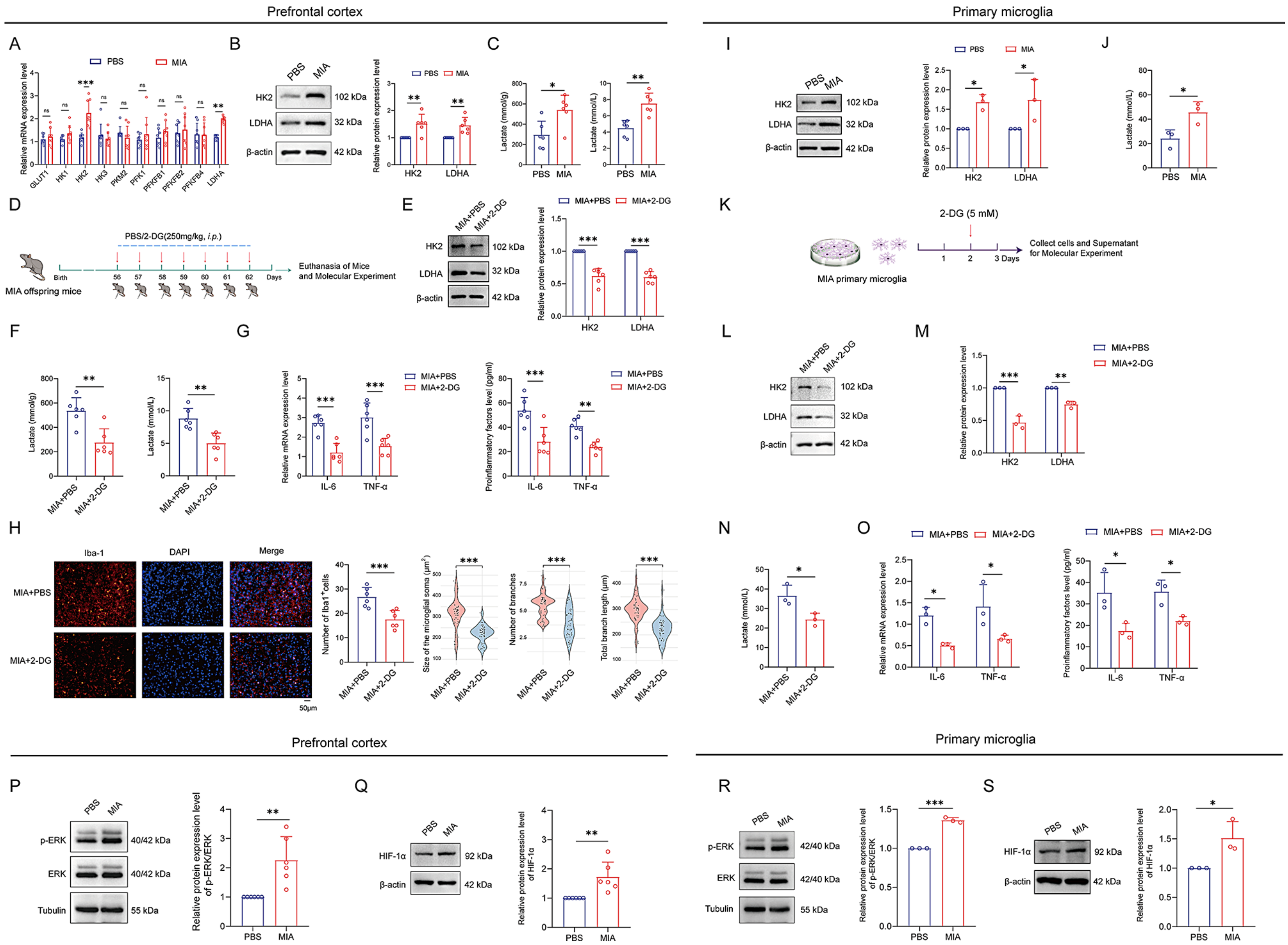

Fig. 4 The activation level of the ERK/HIF-1α pathway and glycolysis were elevated in the MIA offspring mice. (**A**-**B**) The expression of glycolysis key genes of PFC by qPCR (*n*=8) and western blot (*n*=6) between the PBS and MIA offspring mice. Two-way ANOVA. (**C**) Lactate level in the PFC and serum between the PBS and MIA offspring mice. *n*=6. Student's *t*-test. (**D**) Schematic diagram illustrating the experimental procedure of 2-DG administration. (**E**) Western blot analysis of HK2 and LDHA in PFC in MIA offspring mice after 2-DG administration. *n*=6. Two-way ANOVA. (**F**) Lactate level of the PFC and serum in MIA offspring mice after 2-DG administration. *n*=6. Student's *t*-test. (**G**) IL-6 and TNF-α level of PFC and serum in MIA offspring mice after 2-DG administration. *n*=6. Two-way ANOVA. (**H**) Immunostaining analysis of Iba-1$^+$ of PFC in MIA offspring mice after 2-DG administration. Scale bar = 50 μm. Student's *t*-test. (**I**) Western blot analysis of HK2 and LDHA in microglia between the PBS and MIA offspring mice. *n*=3. Two-way ANOVA. (**J**) Lactate level of microglia supernatant between the PBS and MIA offspring mice. *n*=3. Student's *t*-test. (**K**) Schematic diagram of 2-DG intervention for primary microglia from MIA offspring mice. (**L**-**M**) Western blot analysis of HK2 and LDHA in primary microglia with 2-DG intervention. *n*=3. Two-way ANOVA. (**N**) Lactate level of primary microglia supernatant with 2-DG intervention. *n*=3. Student's *t*-test. (**O**) IL-6 and TNF-α level of primary microglia with 2-DG intervention. *n*=3. Two-way ANOVA. (**P**-**S**) Western blot analysis of p-ERK/ERK and HIF-1α of PFC (*n*=6) and primary microglia (*n*=3) between PBS and MIA offspring mice. Student's *t*-test. ns $P \geq 0.05$, *$P<0.05$, **$P<0.01$, ***$P<0.001$

MSC-EVs intervention, suggesting an improvement in cognitive ability (Fig. 5G).

MSC-EVs could inhibit the activation of microglial and Glycolysis in MIA offspring mice

We administered DiI-labeled 100 μg MSC-EVs intranasally into the brains of MIA offspring mice. After 6 h, the DiI-labeled MSC-EVs were significantly enriched in the PFC of the mice, indicating that MSC-EVs could be accumulated in brain tissue via intranasal administration (Fig. 5H, Figure S7).

The MSC-EVs could be successfully delivered to the mouse brain through intranasal administration, increasing the expression level of PD-L1 in the CNS, but without affecting PD-1 expression (Fig. 5I). Moreover, after one-week treatment of MSC-EVs, the IL-6 and TNF-α level in the PFC and serum were significantly reduced (Fig. 5J). As shown in Fig. 5K, in MIA + MSC-EVs group, the level of Iba-1$^+$, the size of the microglial soma, the number of branches, and the total branch length of microglia were all significantly decreased compared to MIA + PBS group. The results above indicated that MSC-EVs could inhibit neuroinflammatory response in the PFC of MIA offspring mice.

Next, we co-cultured MSC-EVs labeled with DiI with primary microglia from the PFC of MIA offspring mice

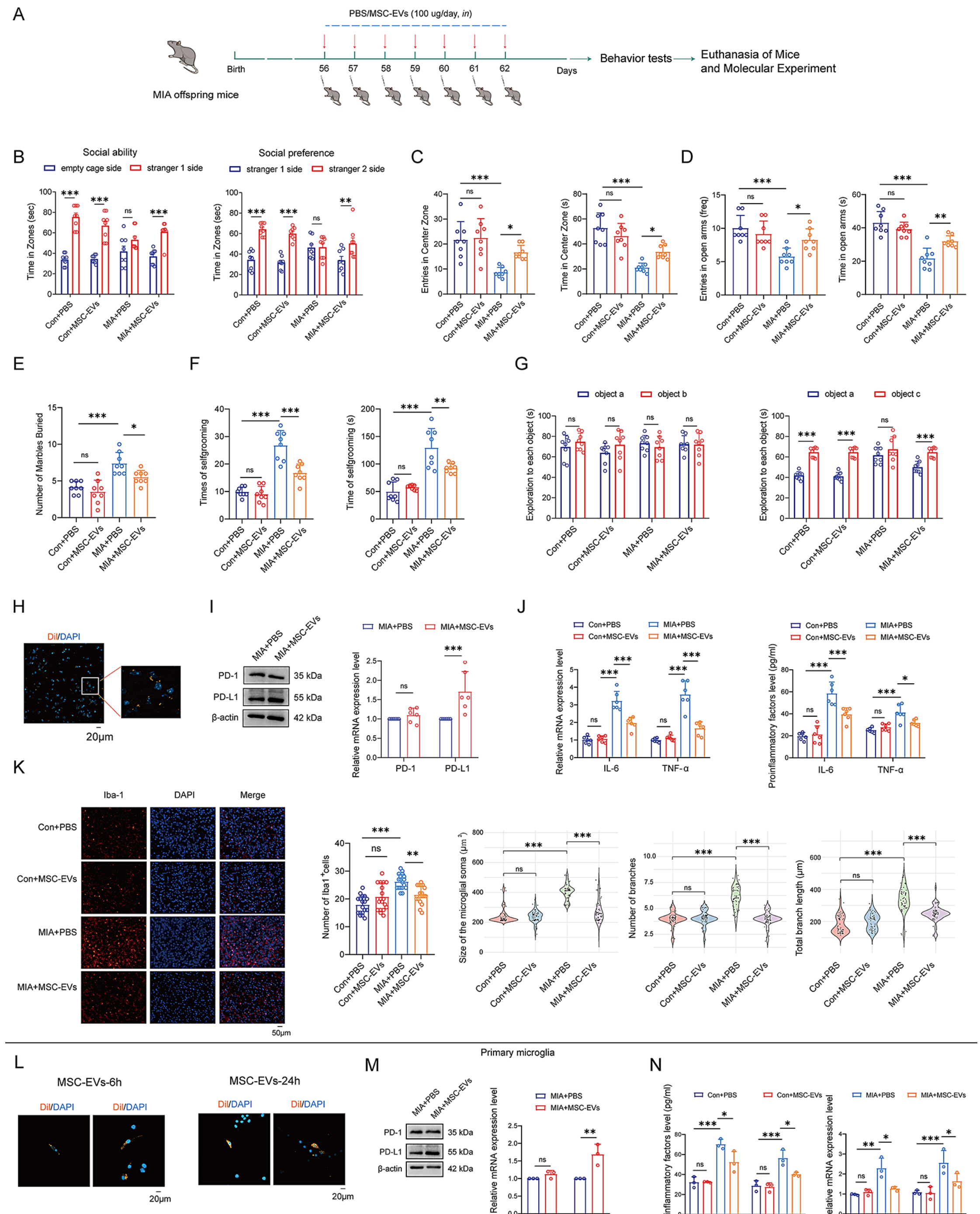

Fig. 5 MSC-EVs alleviated neuroinflammation and autism-like behaviors of MIA offspring mice. (**A**) Schematic diagram illustrating the experimental procedure of MSC-EVs administration. (**B**-**G**) Autism-behaviors analysis between PBS and MIA offspring mice after MSC-EVs administration. (**B**) Statistical chart of sociability and social preference in the three-chamber test. Two-way ANOVA; (**C**) Statistical chart of entries times in center zone and time in center zone in the OFT. One-way ANOVA; (**D**) Statistical chart of entries in open arms and time in open arms in EPM test. One-way ANOVA; (**E**) Statistical chart of number in marbles buried. One-way ANOVA; (**F**) Statistical chart of grooming times and duration of grooming. One-way ANOVA; (**G**) Statistical chart of exploration time for each object in the NOR test. Two-way ANOVA. *n*=8. (**H**) Co-localization of Dil-labeled MSC-EVs of PFC in MIA offspring mice. Scale bar = 20 μm. (**I**) Western blot analysis of PD-1 and PD-L1 of PFC in MIA offspring mice after MSC-EVs administration. *n*=6. Two-way ANOVA. (**J**) IL-6 and TNF-α level of PFC and serum between PBS and MIA offspring mice after MSC-EVs administration. *n*=6. Two-way ANOVA. (**K**) Immunostaining analysis of Iba-1^{+} of PFC between PBS and MIA offspring mice after MSC-EVs administration. Scale bar = 50 μm. One-way ANOVA. (**L**) Co-localization of primary microglia with Dil-labeled MSC-EVs. Scale bar = 20 μm. (**M**) Western blot analysis of PD-1 and PD-L1 of primary microglia in MIA offspring mice with MSC-EVs intervention. *n*=3. Two-way ANOVA. (**N**) IL-6 and TNF-α level of primary microglia in MIA offspring mice with MSC-EVs intervention. *n*=3. Two-way ANOVA. ns *P*≥0.05, **P*<0.05, ***P*<0.01, ****P*<0.001

to explore the immunomodulatory effects and mechanisms of MSC-EVs on microglia. Initially, DiI-labeled MSC-EVs were co-cultured with primary microglia, and MSC-EVs labeled with orange fluorescence were successfully internalized by primary microglia (Fig. 5L).

After 24 h of co-culture, as shown in Fig. 5M, compared to the PBS group, the level of PD-L1 were significantly increased in the MSC-EVs group, while the level of PD-1 showed no significant change. After 48 h of MSC-EVs intervention, the expression level of IL-6 and TNF-α in control group microglia remained unaffected, whereas MSC-EVs significantly reduced the expression of IL-6 and TNF-α in MIA offspring mice (Fig. 5N).

Following the administration of MSC-EVs, the activity of the ERK/HIF-1α pathway was diminished. In the MSC-EVs treated group, the expression level of HK2 and LDHA in the PFC tissue of MIA offspring mice were significantly decreased, as were the level of lactate in both the PFC and serum (Fig. 6A-D). These findings suggested that MSC-EVs could effectively inhibit glycolysis in the PFC of MIA offspring mice.

Following MSC-EVs administration, there was a significant decrease in the expression level of HK2 and LDHA in the PFC microglia of MIA offspring mice, as well as in lactate level in microglia culture supernatant. Moreover, MSC-EVs could inhibit the activity of the ERK/HIF-1α pathway (Fig. 6E-H), suggesting that MSC-EVs may suppress the activation of the ERK/HIF-1α pathway in microglia, thereby reduce cellular glycolysis level, subsequently inhibit the production of inflammatory factors.

MSC-EVs inhibit Glycolysis and neuroinflammation via the PD-L1/PD-1 pathway

To investigate the effect of PD-L1 carried by MSC-EVs on MIA offspring mice, PD-1 Ab was injected into the PFC of MIA offspring mice using brain stereotactic apparatus. Then, MSC-EVs were delivered into brain by intranasal administration daily for 7 days (Fig. 7A).

In PD-1 Ab group, In the EPM test, duration in the open arms was significantly decreased, while, the duration in the closed arms was increased; and the number in marbles buried was increased; while social ability, social preference and cognitive level were not significant difference comparing with the IgG control group (Fig. 7B-G, Figure S8). Moreover, in PD-1 Ab group, the expression of IL-6, TNF-α, p-ERK/ERK, HIF-1α, HK2, LDHA and lactate were all elevated in the PFC and primary microglia, comparing with the IgG control group (Fig. 8A-N). Moreover, the level of Iba-1$^+$, the microglial soma size, branch number, and total branch length were significantly increased in PD-1 Ab group (Fig. 8B). Overall, pharmacological blockade of PD-1 enhanced neuroinflammation, glycolysis and anxiety, repetitive stereotype behaviors in MIA offspring mice.

In addition, in PD-1 Ab + MSC-EVs group, the three-chamber test indicated that both social ability and social preference were decreased; the OFT test showed that entries times and duration in the center zone were significantly reduced; In the EPM test, entries times and duration into the open arms and the number of zone transition were significantly decreased, while the duration in the closed arms was increased; the number in marbles buried, grooming times and duration were all increased; the NOR test indicated cognitive level was decreased, comparing with the IgG + MSC-EVs group (Fig. 7B-G). Moreover, in PD-1 Ab + MSC-EVs group, the expression of IL-6, TNF-α, Iba-1, p-ERK/ERK, HIF-1α, HK2, LDHA and lactate were all elevated in the PFC and primary microglia, while the expression of PD-1 was no significant changed, comparing with the IgG + MSC-EVs group (Fig. 8A-N). Furthermore, comparing with the IgG + MSC-EVs control group, the level of Iba-1$^+$, the microglial soma size, branch number, and total branch length were all elevated in the PD-1 Ab + MSC-EVs group. Overall, pharmacological blockade of PD-L1/PD-1 weakened the effect of MSC-EVs on neuroinflammation, glycolysis and autism-like behaviors in MIA offspring mice.

To further verify the effect of PD-L1 carried by MSC-EVs on MIA offspring mice, AAV-Iba-1-shPdcd1 was injected into the PFC of MIA offspring mice using brain stereotactic apparatus. Three weeks later, MSC-EVs were delivered into brain by intranasal administration daily for 7 days (Fig. 9A). In AAV-Iba-1-shPdcd1 + MSC-EVs group, the three-chamber test indicated that both social ability and social preference were decreased; the OFT test showed that entries times and duration in the center zone were significantly reduced; In the EPM test, entries times and duration into the open arms and the number of zone transition were significantly decreased, while the duration in the closed arms was increased; the number in marbles buried, grooming times and duration were all increased; the NOR test indicated cognitive level was decreased, comparing with the AAV-Ctrl + MSC-EVs group (Fig. 9B-G, Figure S9). Moreover, in AAV-Iba-1-shPdcd1 + MSC-EVs group, the expression of IL-6, TNF-α, Iba-1, p-ERK/ERK, HIF-1α, HK2, LDHA and lactate were all elevated in the PFC and serum, while the expression of PD-1 was decreased, comparing with the AAV-Ctrl + MSC-EVs group (Fig. 9H-O). Overall, microglia-specific PD-1 knockdown weakened the effect of MSC-EVs on neuroinflammation, glycolysis and autism-like behaviors in MIA offspring mice.

Nextly, we reconfirmed whether PD-1 participates in the regulation on neuroinflammation and glycolysis in microglia by transfecting them with siRNA targeting

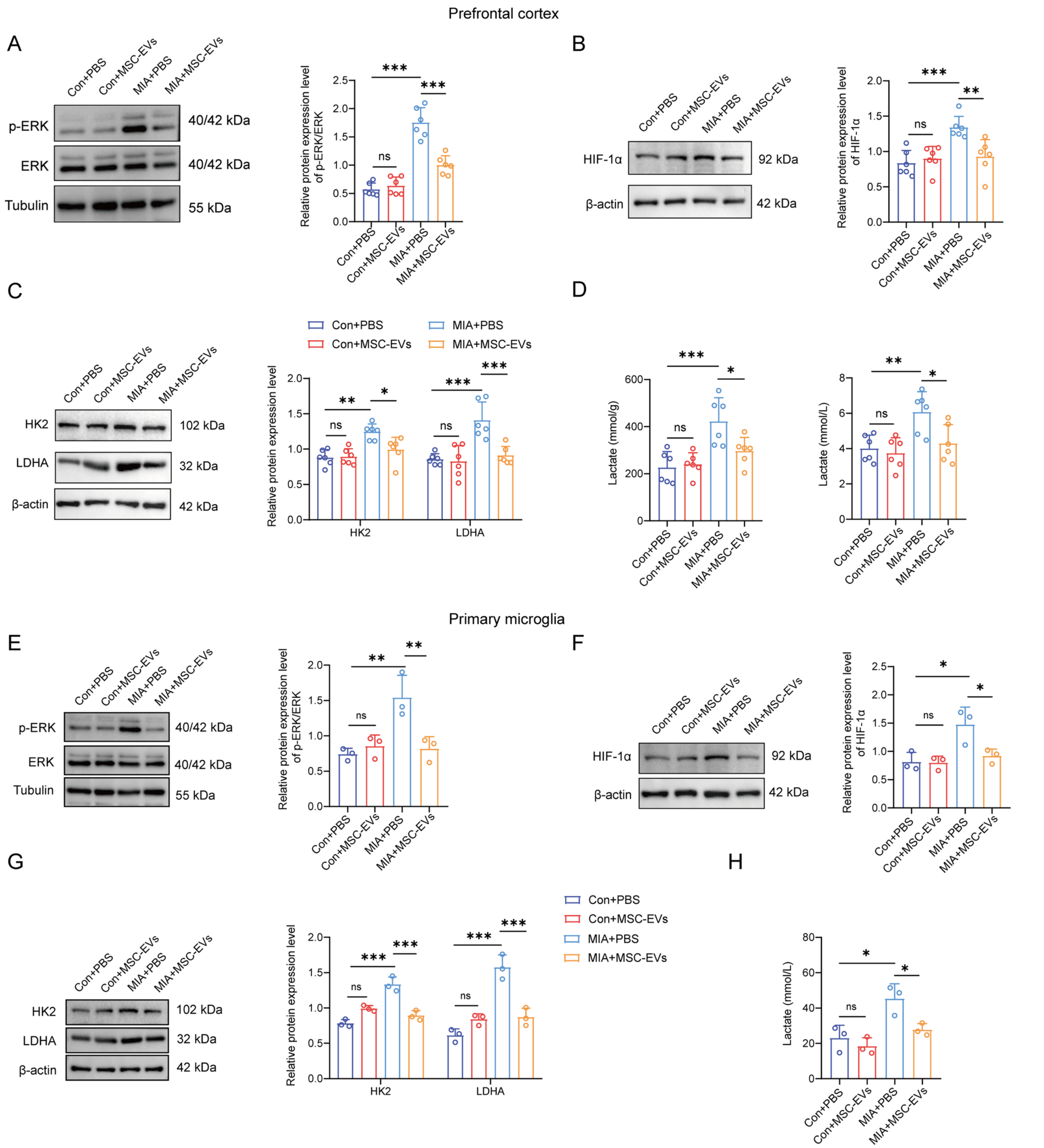

Fig. 6 MSC-EV repressed the glycolysis process in MIA offspring mice. (**A**-**C**) Western blot analysis of p-ERK/ERK, HIF-1α, HK2 and LDHA of PFC between PBS and MIA offspring mice after MSC-EVs administration. *n*=6. One-way ANOVA, Two-way ANOVA. (**D**) Lactate level of PFC and serum between PBS and MIA offspring mice after MSC-EVs administration. *n*=6. One-way ANOVA. (**E**-**G**) Western blot analysis of p-ERK/ERK, HIF-1α, HK2 and LDHA in primary microglia with MSC-EVs intervention. *n*=3.One-way ANOVA, Two-way ANOVA. (**H**) Lactate level in primary microglia supernatant with MSC-EVs intervention. *n*=3. One-way ANOVA. ns $P \geq 0.05$, *$P<0.05$, **$P<0.01$, ***$P<0.001$

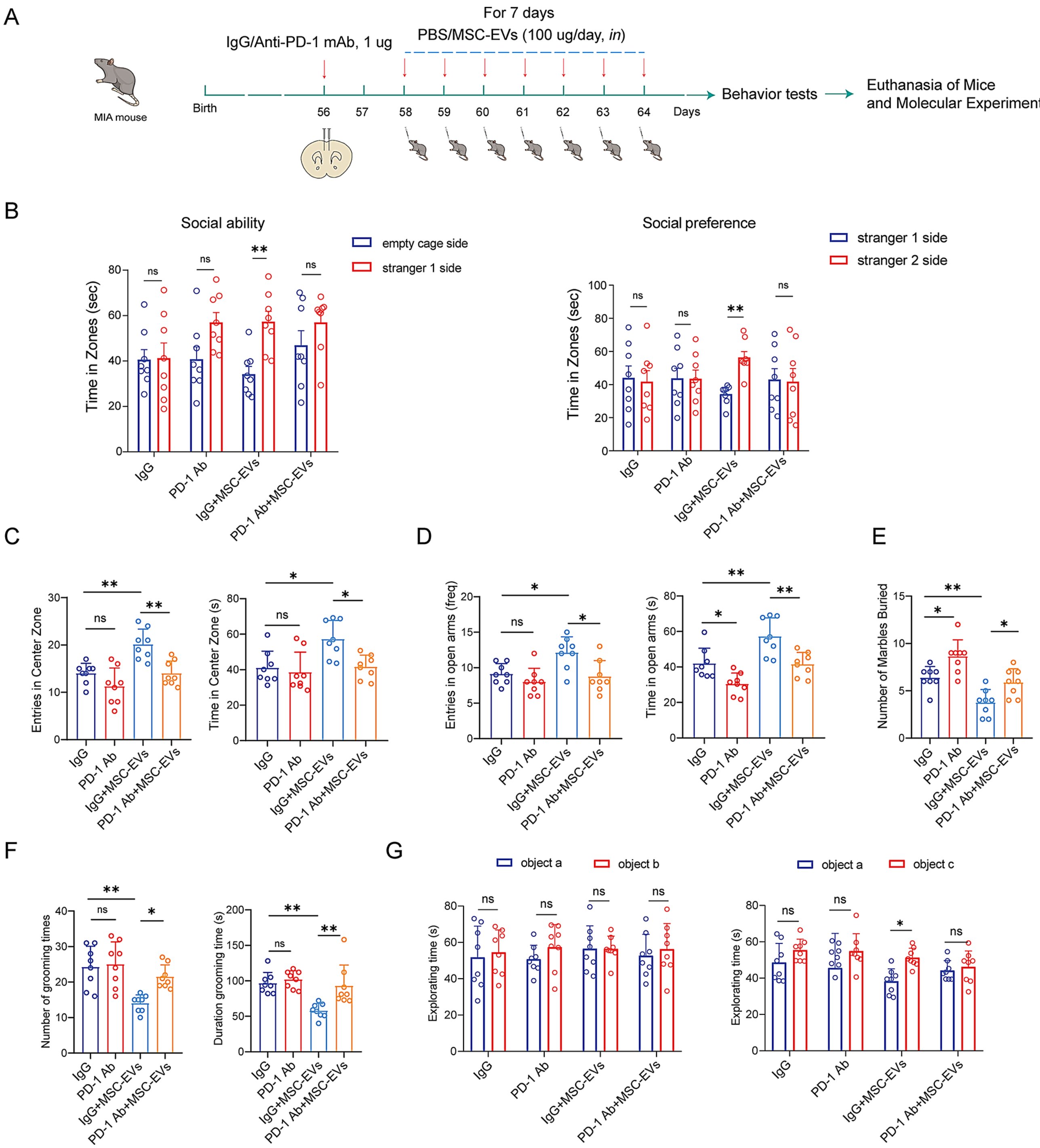

Fig. 7 Pharmacological blockade of PD-1 weakened the effect of MSC-EVs on improving autism-like behaviors in MIA offspring mice. (**A**) Schematic diagram illustrating the experiment procedure of MIA offspring mice after PD-1 Ab alone or PD-1 Ab + MSC-EVs administration. (**B**-**G**) Autism-behaviors analysis of MIA offspring mice after PD-1 Ab alone or PD-1 Ab + MSC-EVs administration. (**B**) Statistical chart of sociability and social preference in the three-chamber test. Two-way ANOVA; (**C**) Statistical chart of entries times in center zone and time in center zone in the OFT. One-way ANOVA; (**D**) Statistical chart of entries in open arms and time in open arms in EPM test. One-way ANOVA; (**E**) Statistical chart of number in marbles buried. One-way ANOVA; (**F**) Statistical chart of grooming times and duration grooming. One-way ANOVA; (**G**) Statistical diagram of exploration time for each object in the NOR test. Two-way ANOVA. *n*=8. ns *P*≥0.05, **P*<0.05, ***P*<0.01, ****P*<0.001

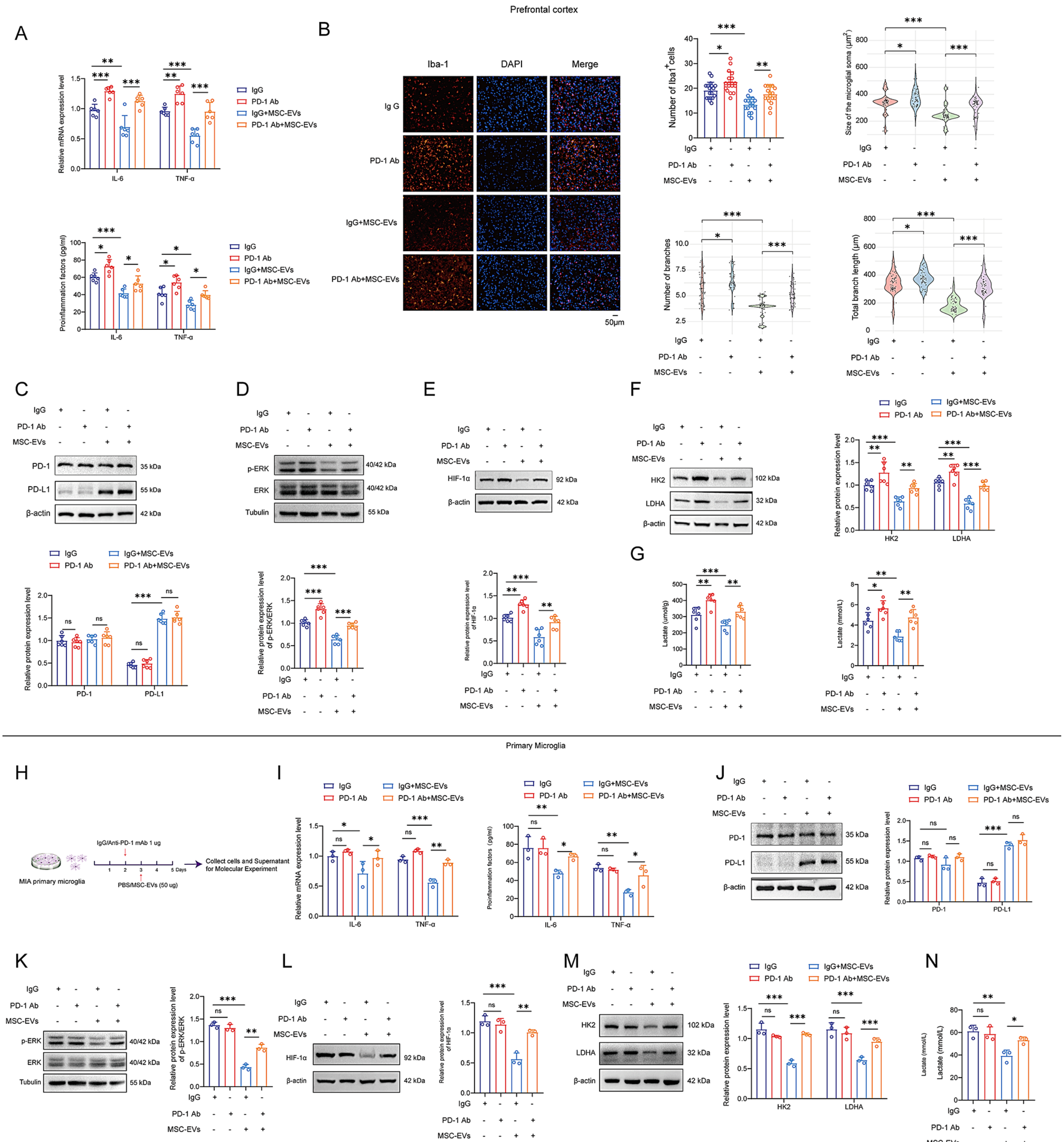

Fig. 8 Pharmacological blockade of PD-1 weakened the effect of MSC-EVs on neuroinflammation and glycolysis in MIA offspring mice. (**A**) IL-6 and TNF-α level of PFC and serum in MIA offspring mice after PD-1 Ab alone or PD-1 Ab + MSC-EVs administration. *n*=6. Two-way ANOVA. (**B**) Immunostaining analysis of Iba-1$^+$ of PFC in MIA offspring mice after PD-1 Ab alone or PD-1 Ab + MSC-EVs administration. Scale bar = 50 μm. One-way ANOVA. (**C**-**F**) Western blot analysis of PD-1, PD-L1, p-ERK/ERK, HIF-1α, HK2 and LDHA of PFC in MIA offspring mice after PD-1 Ab alone or PD-1 Ab + MSC-EVs administration. *n*=6. One-way ANOVA, Two-way ANOVA. (**G**) Lactate level of PFC and serum in MIA offspring mice after PD-1 Ab alone or PD-1 Ab + MSC-EVs administration. *n*=6. One-way ANOVA. (**H**) Schematic diagram illustrating the experiment procedure of with PD-1 Ab alone or PD-1 Ab + MSC-EVs intervention in primary microglia. (**I**) IL-6 and TNF-α level of primary microglia with PD-1 Ab alone or PD-1 Ab + MSC-EVs intervention. *n*=3. Two-way ANOVA. (**J**-**M**) Western blot analysis of PD-1 and PD-L1. p-ERK/ERK, HIF-1α, HK2 and LDHA in primary microglia after PD-1 Ab alone or PD-1 Ab + MSC-EVs intervention. *n*=3. One-way ANOVA, Two-way ANOVA. (**N**) Lactate level in primary microglia supernatant after PD-1 Ab alone or PD-1 Ab + MSC-EVs intervention. *n*=3. One-way ANOVA. ns *P*≥0.05, **P*<0.05, ***P*<0.01, ****P*<0.001

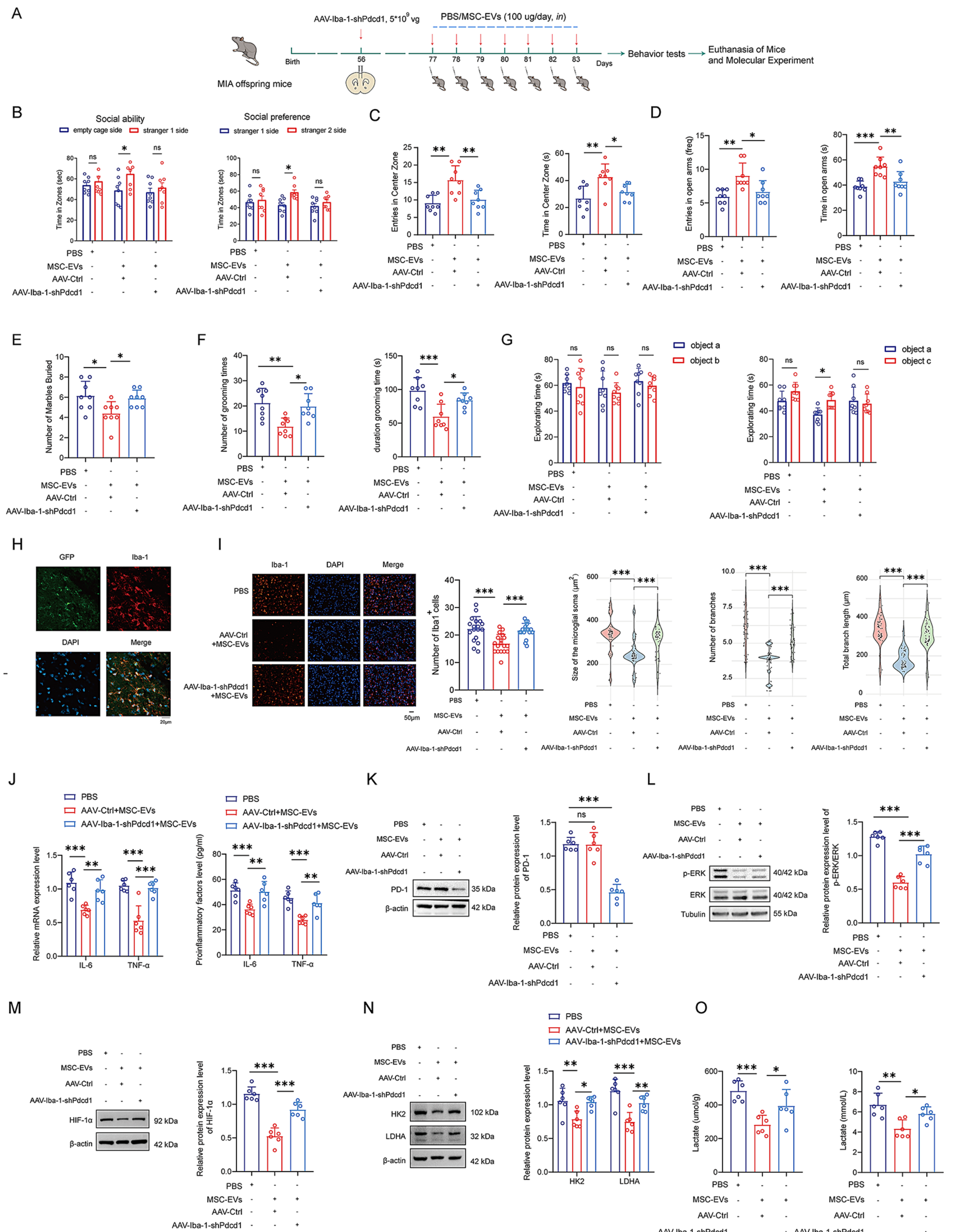

Fig. 9 Microglia-specific PD-1 knockdown repressed the effect of MSC-EVs on inhibiting neuroinflammation, glycolysis and autism-like behaviors in MIA offspring mice. (**A**) Schematic diagram illustrating the experimental procedure of MIA offspring mice after Ctrl + MSC-EVs or AAV-Iba-1-shPdcd1 + MSC-EVs administration. (**B**-**G**) Autism-behaviors analysis of MIA offspring mice after Ctrl + MSC-EVs or AAV-Iba-1-shPdcd1 + MSC-EVs administration. (**B**) Statistical chart of sociability and social preference in the three-chamber test. Two-way ANOVA; (**C**) Statistical chart of entries times in center zone and time in center zone in the OFT. One-way ANOVA; (**D**) Statistical chart of entries in open arms and time in open arms in EPM test. One-way ANOVA; (**E**) Statistical chart of number in marbles buried. One-way ANOVA; (**F**) Statistical chart of grooming times and duration grooming. One-way ANOVA; (**G**) Statistical diagram of exploration time for each object in the NOR test. Two-way ANOVA. (**H**) Immunostaining analysis of GFP^{+} cells stained with Iba-1^{+}. Scale bar: 20 µm. (**I**) Immunostaining analysis of Iba-1^{+} of PFC in MIA offspring mice after Ctrl + MSC-EVs or AAV-Iba-1-shPdcd1 + MSC-EVs administration. Scale bar = 50 µm. One-way ANOVA. (**J**) IL-6 and TNF-α level of PFC and serum in MIA offspring mice after Ctrl + MSC-EVs or AAV-Iba-1-shPdcd1 + MSC-EVs administration. *n*=6. Two-way ANOVA. (**K**-**N**) Western blot analysis of PD-1, PD-L1, p-ERK/ERK, HIF-1α, HK2 and LDHA of PFC in MIA offspring mice after Ctrl + MSC-EVs or AAV-Iba-1-shPdcd1 + MSC-EVs administration. *n*=6. One-way ANOVA, Two-way ANOVA. (**O**) Lactate level of PFC and serum in MIA offspring mice after Ctrl + MSC-EVs or AAV-Iba-1-shPdcd1 + MSC-EVs administration. *n*=6. One-way ANOVA. ns $P \geq 0.05$, *$P<0.05$, **$P<0.01$, ***$P<0.001$

Pdcd1 (siRNA-Pdcd1). Knocking down Pdcd1 in microglia inhibited expression of PD-1, p-ERK/ERK, HIF-1α, IL-6 and TNF-α, and glycolysis-related proteins HK2 and LDHA, which were similar to that showed upon PD-1 pharmacological inhibition (Fig. 10). In conclusion, our data indicated that MSC-EVs downregulates ERK/HIF-1α signaling to suppress neuroinflammation and elevated glycolysis in microglia.

To discern the effect of PD-L1 derived from MSC-EVs on neuroinflammation, glycolysis and autism-like behaviors in MIA offspring mice, we constructed engineering modified MSC-EVs with PD-L1 deficient through

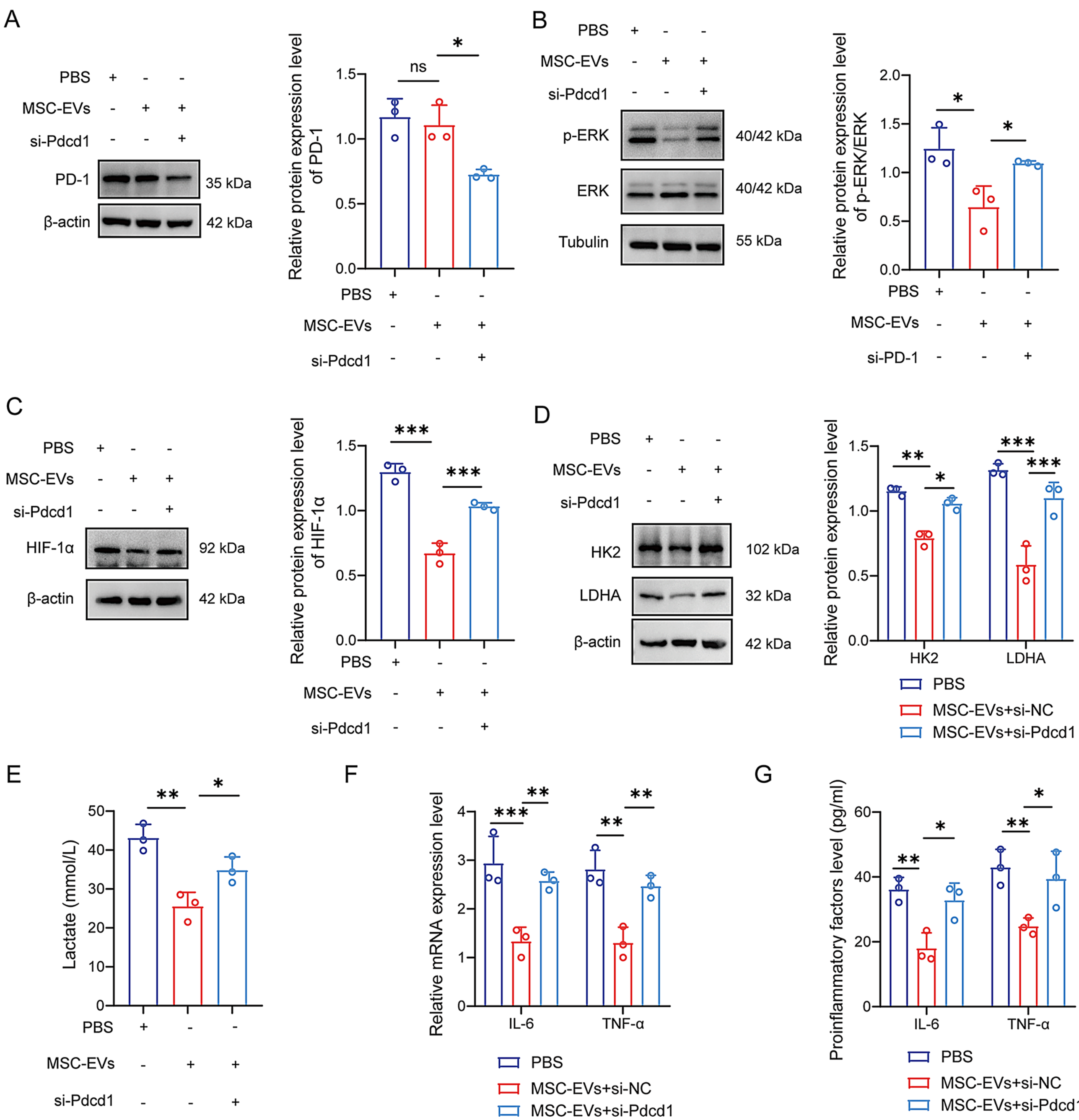

Fig. 10 Genetic suppression of PD-1 weakened the effect of MSC-EVs on neuroinflammation and glycolysis in MIA offspring mice. (**A**-**D**) Western blot analysis of PD-1, p-ERK/ERK, HIF-1α, HK2 and LDHA in primary microglia with MSC-EVs + si-Pdcd1 intervention. *n*=3. One-way ANOVA, Two-way ANOVA. (**E**) Lactate level in primary microglia supernatant with MSC-EVs + si-Pdcd1 intervention. *n*=3. One-way ANOVA. (**F**-**G**) IL-6 and TNF-α level of primary microglia with MSC-EVs + si-Pdcd1 intervention. *n*=3. Two-way ANOVA.ns $P \geq 0.05$, *$P<0.05$, **$P<0.01$, ***$P<0.001$

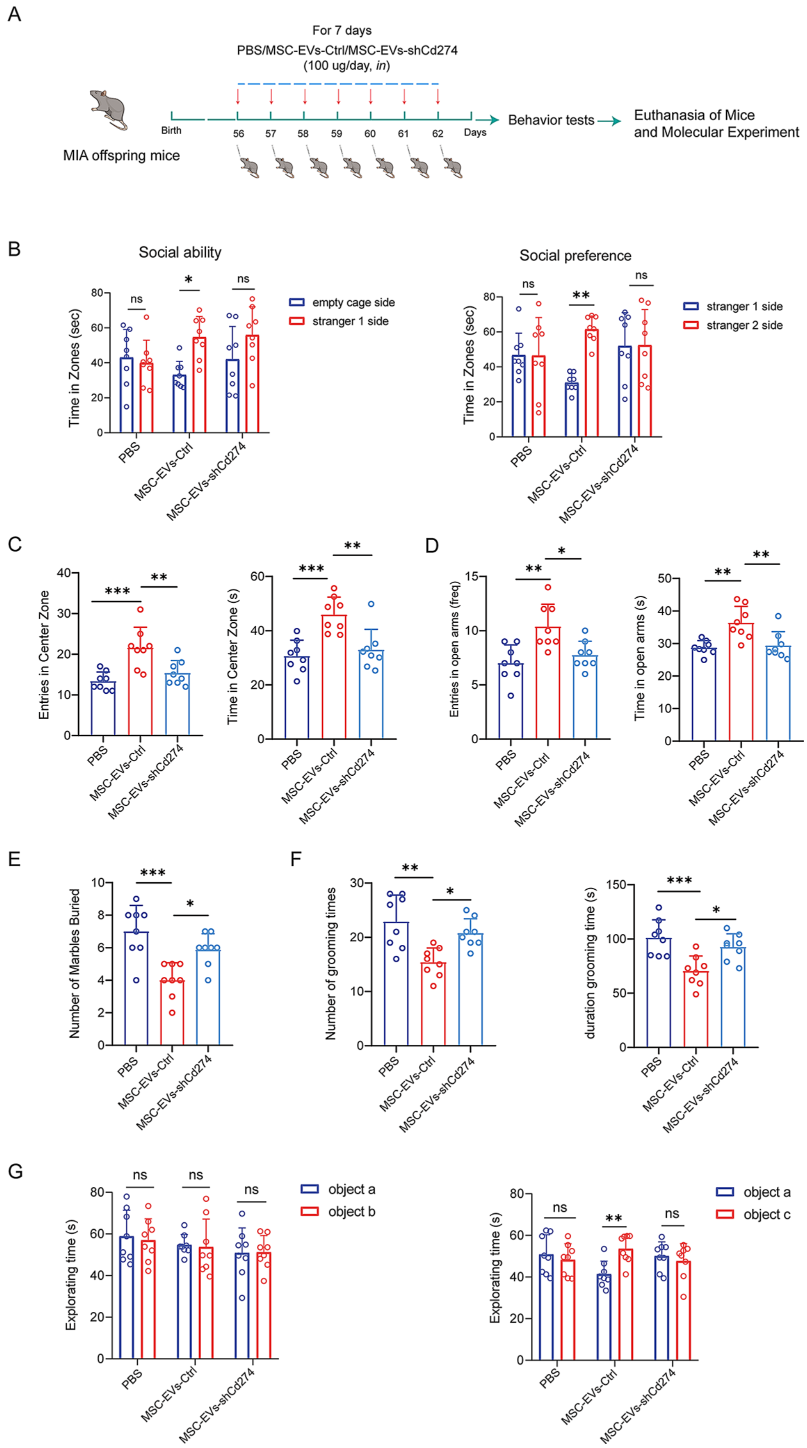

Fig. 11 MSC-EVs with PD-L1 knockdown weakened the effect on autism-like behaviors in MIA offspring mice. (**A**) Schematic diagram illustrating the experiment procedure of MIA offspring mice after MSC-EVs-Ctrl or MSC-EVs-shCd274 administration. (**B**-**G**) Autism-behaviors analysis of MIA offspring mice after MSC-EVs-Ctrl or MSC-EVs-shCd274 administration. (**B**) Statistical chart of sociability and social preference in the three-chamber test. Two-way ANOVA; (**C**) Statistical chart of entries times in center zone and time in center zone in the OFT. One-way ANOVA; (**D**) Statistical chart of entries in open arms and time in open arms in EPM test. One-way ANOVA; (**E**) Statistical chart of number in marbles buried. One-way ANOVA; (**F**) Statistical chart of grooming times and duration grooming. One-way ANOVA; (**G**) Statistical diagram of exploration time for each object in the NOR test. Two-way ANOVA. n=8. ns $P \geq 0.05$, *$P<0.05$, **$P<0.01$, ***$P<0.001$

transfecting shCd274 lentivirus (Figure S10). Then, MSC-EVs-Ctrl or MSC-EVs-shCd274 were delivered into MIA offspring brain by intranasal administration daily for 7 days (Fig. 11A). Behavior tests showed the social ability, social preference, anxiety and repetitive stereotyped behaviors were still presented in MSC-EVs-shCd274 group (Fig. 11B-G, Figure S11). In addition, the PD-L1 of PFC in MSC-EVs-shCd274 group were obviously less than MSC-EVs-Ctrl group. Comparing with MSC-EVs-Ctrl group, the expression of p-ERK/ERK, HIF-1α, HK2, LDHA, IL-6, TNF-α and lactate were all significantly increased in MSC-EVs-shCd274 group. Therefore, PD-L1 deficient weakened the effect of MSC-EVs on neuroinflammation, glycolysis and autism-like behaviors in MIA offspring mice (Fig. 12A-G). In vitro, MSC-EVs-Ctrl or MSC-EVs-shCd274 were co-cultured with MIA primary microglia. As illustrated in Fig. 12H-N, in the MSC-EVs-shCd274 group, the expression of p-ERK/ERK, HIF-1α, HK2, and LDHA, IL-6, TNF-α and lactate were all significantly increased comparing with MSC-EVs-Ctrl group. In summary, PD-L1-deficient MSC-EVs diminished the protective effect of MSC-EVs on neuroinflammation and glycolysis in MIA primary microglia.

To futher investigated the association of ERK and HIF-1α in primary microglia of MIA offspring mice, we used honokiol, a specific activator of ERK, and SL327, a specific inhibitor of ERK. In contrast, pretreatment with 20 μM honokiol markedly induced MSC-EVs inhibited HIF-1α expression and glycolysis (Fig. 13A-F). Moreover, pretreatment with 10 μM SL327 markedly decreased MSC-EVs combined PD-1 Ab-induced HIF-1α expression and glycolysis (Fig. 13G-L), indicating that HIF-1α-induced glycolysis were regulated by ERK activation in microglia.

Discussion

The neuroinflammatory response of microglia, which was triggered by stimulation and damage, could aggravate brain damage, affect brain development, and ultimately cause inflammatory CNS diseases [28–30]. More evidences support that MIA induced by maternal infections, allergies or autoimmune diseases, was one of the significant risk factors of ASD [2]. It is worth emphasizing that the infectious agents can not injure the fetal brain directly, but they induce microglial activation and enhance immune response in the offspring by increasing pro-inflammatory cytokine level in both brain and peripheral serum in response to exogenous stimulation [6, 31–34]. More importantly, the cytokines and chemokines were elevated at different developmental stages and continued to develop into adulthood in MIA models, which eventually leading to neurodevelopmental disorders [35]. In this study, we found that MIA offspring mice exhibited classic autism-like behaviors, and an increase in the number of microglia. Moreover, IL-6 and TNF-α were elevated significantly, not only in the fetal brain but also PFC and peripheral serum in adulthood offspring. All these results indicated that neuroinflammation was closely associated with the pathogenesis of ASD.

Recent studies showed there was abnormally increasing lactate and LDHA in ASD patients [36–39]. Hideo et al. [40] also reported that ASD patients exhibited high lactate level, consequently along with the brain pH decreased. Furthermore, this phenomenon was also observed in several kinds of ASD mice models. Licznerski et al. [41] have found significant upregulation of HK1, HK2, PFKP, PKM2 and LDHA, which were all glycolysis-related key enzymes in *Fmr1*$^{-/-}$ mice. Similarly, significantly increased glycolysis level were also observed in the PFC of *Shank3B*$^{-/-}$ mice and VPA induced mice models. It has also been reported that the some ASD behaviors could be rescued when suppressnig the glycolysis by 2-DG in VPA-induced mice [42]. Thus, the clinical reports and mice research above have inspired the importance of "Warburg effect hypothesis" in ASD pathology, indicating that rising glycolysis may be one risk factor for ASD [43]. Our research showed that the lactate level were all elevated in the supernatant of primary microglia, PFC and peripheral serum from MIA offspring mice, at the same time, along with the increasing expression of glycolysis key enzymes (HK2 and LDHA).

Furthermore, active microglia were typically involved in a metabolic reprogramming, mainly manifested in increased glycolysis, so as to provide energy rapidly. Microglia stimulated by LPS could induce fierce inflammtory response, with the glucose consumption and lactate production. While, supressing glycolysis could also eliminate LPS-induced microglial activation via NF-κB pathway [44]. Thereby, these research findings have demonstrated that neuroinflammation can enhance glycolysis in the neurometabolism process. Conversely, it is an available way to downregulate inflammation activation by inhibiting the glycolysis. Here, IL-6, TNF-α and lactate level were all decreased in primary microglia and PFC of MIA offspring mice, upon interventing with the glycolysis inhibitor 2-DG. This study suggested that glucose metabolism may be a key regulatory factor in neurological inflammation, which broadening the avenue in treating inflammation-related diseases by manipulating the metabolism of immune cells.

Remarkably, several evidences have showed that MSC-EVs exhibited significant therapeutic potential in various neurodevelopmental disorders through inhibiting neuroinflammation. Previous studies demonstrated that MSC-EVs pocessed the anti-inflammatory properties and facilitated neuroregeneration and angiogenesis when applied for ischemic stroke [45]. Allaura et al. [46] have

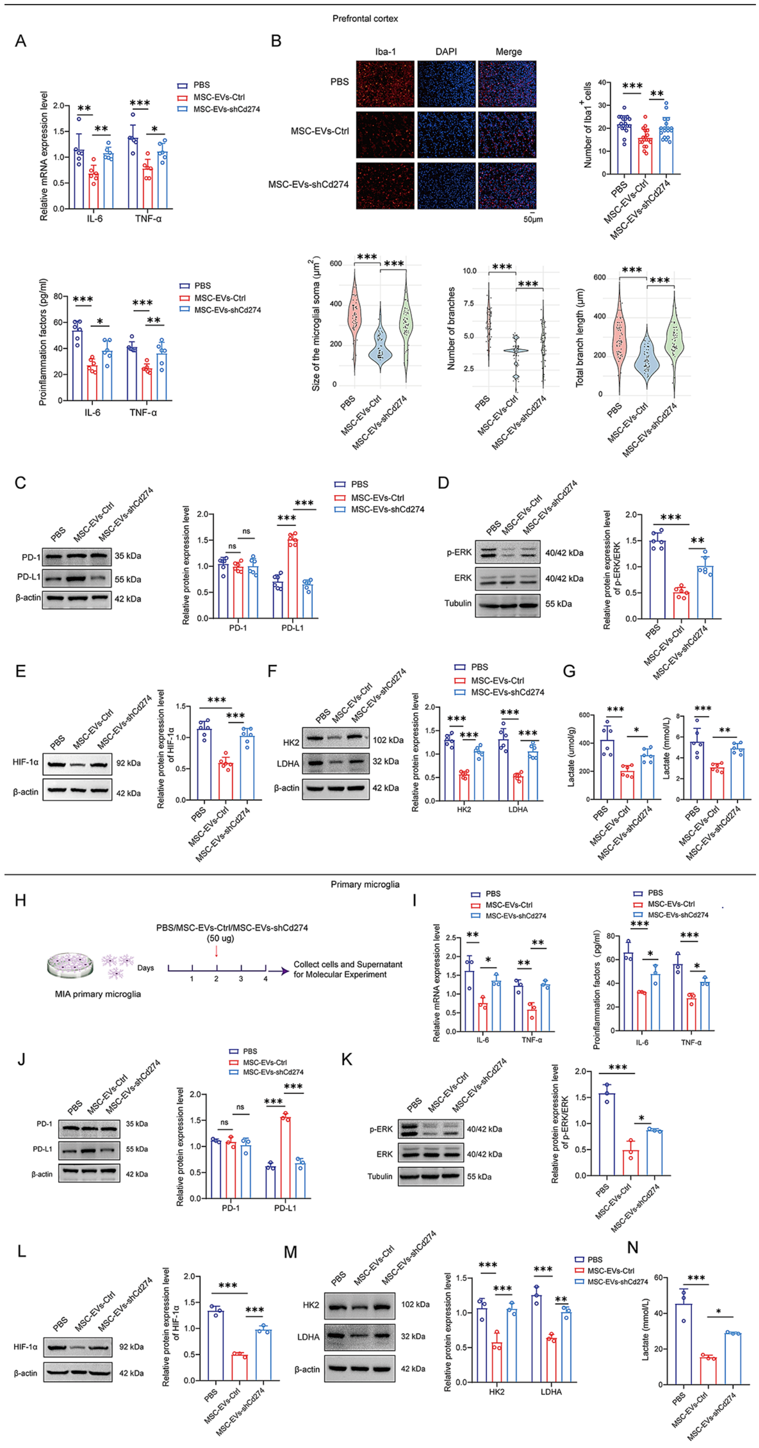

Fig. 12 MSC-EVs with PD-L1 knockdown weakened the effect on neuroinflammation and glycolysis in MIA offspring mice. (**A**) IL-6 and TNF-α level of PFC and serum in MIA offspring mice after MSC-EVs-Ctrl or MSC-EVs-shCd274 administration. *n*=6. Two-way ANOVA. (**B**) Immunostaining analysis of Iba-1^{+} of PFC in MIA offspring mice after MSC-EVs-Ctrl or MSC-EVs-shCd274 administration. *n*=6. Scale bar = 50 μm. One-way ANOVA. (**C**-**F**) Western blot analysis of PD-L1/PD-1, p-ERK/ERK, HIF-1α, HK2 and LDHA of PFC in MIA offspring mice after MSC-EVs-Ctrl or MSC-EVs-shCd274 administration. *n*=6. One-way ANOVA, Two-way ANOVA. (**G**) Lactate level of PFC and serum in MIA offspring mice after MSC-EVs-Ctrl or MSC-EVs-shCd274 administration. *n*=6. One-way ANOVA. (**H**) Schematic diagram illustrating the experiment procedure of primary microglia with MSC-EVs-Ctrl or MSC-EVs-shCd274 intervention. (**I**) IL-6 and TNF-α level of primary microglia with MSC-EVs-Ctrl or MSC-EVs-shCd274 intervention. *n*=3. Two-way ANOVA. (**J**-**M**) Western blot analysis of PD-L1/PD-1, p-ERK/ERK, HIF-1α, HK2 and LDHA in primary microglia with MSC-EVs-Ctrl or MSC-EVs-shCd274 intervention. *n*=3. One-way ANOVA, Two-way ANOVA. (**N**) Lactate level of primary microglia supernatant with MSC-EVs-Ctrl or MSC-EVs-shCd274 intervention. *n*=3. One-way ANOVA. ns $P \geq 0.05$, *$P<0.05$, **$P<0.01$, ***$P<0.001$

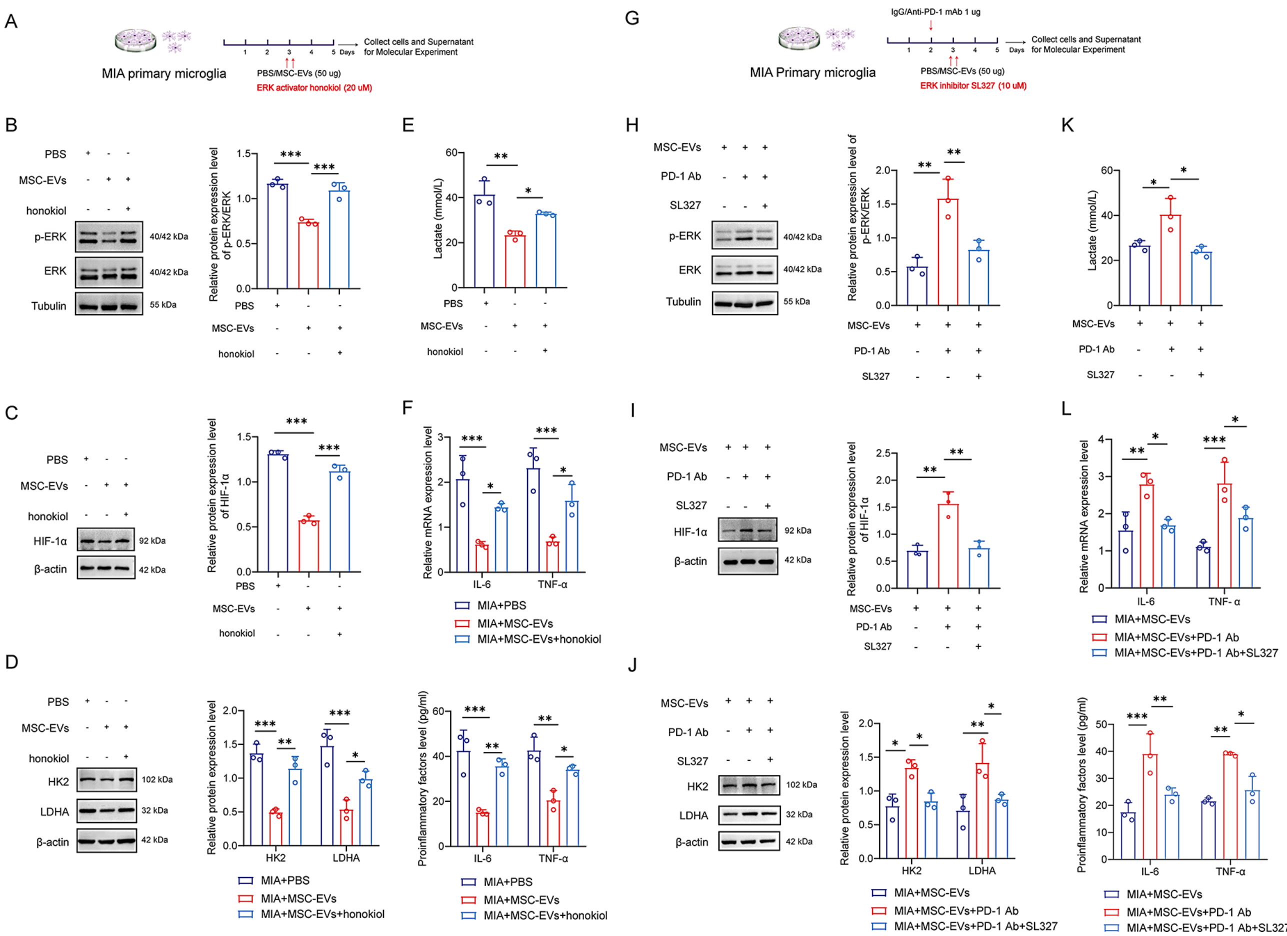

Fig. 13 MSC-EVs inhibited microglial activation and glycolysis via the PD-1/ERK/HIF-1α pathway. (**A**) Schematic diagram illustrating the experiment procedure of combining MSC-EVs with ERK activator honokiol intervention in primary microglia. (**B**-**D**) Western blot analysis of p-ERK, ERK, HIF-1α, HK2 and LDHA in primary microglia with combining MSC-EVs and ERK activator honokiol intervention. *n*=3. One-way ANOVA, Two-way ANOVA. (**E**) Lactate level in primary microglia supernatant with combining MSC-EVs with ERK activator honokiol intervention. *n*=3. One-way ANOVA. (**F**) IL-6 and TNF-α level of primary microglia with combining MSC-EVs with ERK activator honokiol intervention. *n*=3. Two-way ANOVA. (**G**) Schematic diagram illustrating the experiment procedure of MSC-EVs combining PD-1 Ab and ERK inhibitor SL327 intervention in primary microglia. (**H**-**J**) Western blot analysis of p-ERK, ERK, HIF-1α, HK2 and LDHA in primary microglia of MSC-EVs combining PD-1 Ab and ERK inhibitor SL327 intervention. *n*=3. One-way ANOVA, Two-way ANOVA. (**K**) Lactate level of primary microglia supernatant of MSC-EVs combining PD-1 Ab and ERK inhibitor SL327 intervention. *n*=3. One-way ANOVA. (**L**) IL-6 and TNF-α level of primary microglia of MSC-EVs combining PD-1 Ab and ERK inhibitor SL327 intervention. *n*=3. Two-way ANOVA. ns $P \geq 0.05$, *$P<0.05$, **$P<0.01$, ***$P<0.001$

reported that microglial activation was inhibited and release of IL-1β, TNF-α and IL-6 were reduced when intranasally delivering MSC-EVs to Alzheimer mice, futher to improve the recognization behavior of mice. In this study, we found that MSC-EVs could significantly decrease the expression of Iba-1$^+$, IL-6 and TNF-α in the PFC of MIA offspring mice.

PD-1 is a co-inhibitory receptor that interacts with its ligand PD-L1 to inhibit T cell receptor (TCR)-mediated signaling. It is prominently expressed on tumor infiltrating lymphocytes (TILs), while PD-L1 is highly expressed on tumor cells. Therefore, the immune checkpoint PD-L1/PD-1 is an effective method for tumor therapy, as tumor cells utilize regulatory defense mechanisms to evade attacks from immune cells. While the mechanisms of the PD-L1/PD-1 axis have primarily been studied in T cells, there are involved increasingly evidences that other cell types in the CNS. In addition, PD-L1/PD-1 axis has potential ability in reducing neuroinflammatory response and potentially regulating neuronal activity [10]. Zhang et al. [47] showed that PD-L1/PD-1 axis induced M2 polarization of microglia by reducing phosphorylation of STAT1, increasing phosphorylation of STAT6, and then downregulating the NF-κB signaling. Additionally, ERK pathway in microglia was a key regulatory factor in pro-inflammatory response, which could be modulated by PD-L1/PD-1 axis in neuropathic pain [48]. Despite this, research on the relationship between the PD-1/PD-L1 axis and MIA induced ASD is currently limited. Here, we observed that PD-L1 was highly expressed in the MSC and MSC-EVs, the level of PD-1 was upregulated and the ERK pathway was activated in primary microglia and PFC of MIA mice model. MSC-EVs was performed to MIA offspring mice by intranasal delivering or co-cultured with primary microglia, which could significantly elevated PD-L1 level, then activated PD-L1/PD-1 axis, repressed the ERK pathway and futher inhibited the microglia activation and glycolysis. Therefore, we speculated that PD-L1/PD-1 axis has potential ability in decreasing neuroinflammatory response, implicating a possible method for ASD therapy.

HIF-1α is a crucial transcription factor for glucose metabolism by promoting the transcription of the key enzymes in glycolysis (GLUT1, HK2, PKM2 and LDHA) [49, 50]. It is known that the activation of ERK pathway could act as an upstream modulator of HIF-1α and increase the glycolysis in cancer [51]. Our research indicated that ERK/HIF-1α pathway was inhibited by MSC-EVs due to PD-L1/PD-1 axis. More importantly, the effects of MSC-EVs on the neuroinflammation and glycolysis could be weakend by brain stereotaxic injection of PD-1 Ab or microglia-specific PD-1 knockdown via AAV-Iba-1-shPdcd1 in vivo, and trandfected with Pdcd1 siRNA in microglia in vitro. Notably, MSC-EVs with PD-L1 knockdown could also weaken the effect on neuroinflammation, glycolysis and autism-like behaviors of MIA offspring mice. What's more, pharmacological inhibition of ERK could suppress HIF-1α mediated glycolysis and neuroinflammation in primary microglia of MIA offspring mice. While, the ERK activator treatment exacerbate the level of pro-inflammatory factors and latate. All the above experiments have proved that MSC-EVs could maintain glycolysis and immune homeostasis through mediating ERK/HIF-1α and transcription of HK2 and LDHA by PD-L1/PD-1.

MSC-EVs have a protective effect on nerve cells through their various bioactive substances, such as neurotrophic factors, immune regulatory and anti-inflammatory molecules, which can alleviate neuronal damage, inhibit neuronal apoptosis, and maintain the normal structure and function of neurons [52, 53]. Zhao et al. have reported that PD-1 could regulate neuronal excitability in hippocampal neurons, and the selective deletion of PD-1 in excitatory neurons could enhance long-term potentiation (LTP) and memory of mice [54]. Notably, PD-1 was expressed in microglia, astrocytes and neurons by immunostaining in our study, but only in microglia PD-1 was significantly higher than controls. Therefore, we explored that PD-L1 carried by MSC-EVs attenuated neuroinflammation, glycolysis and autism-like behaviors in MIA offspring mice, which activated PD-L1/PD-1 axis in microglia.

Conclusions

In conclusion, based on the immunosuppressive properties of the PD-1/PD-L1 axis, our study explored the potential therapy on MSC-EVs in alleviating MIA-induced ASD in offspring. We identified a critical link between neuroinflammation and hyperactivated glycolysis, both *in vivo* and in vitro, highlighting their contribution to ASD pathogenesis. MSC-EVs effectively alleviated autism-like behaviors by suppressing hyperactivation of microglia and glycolysis through the PD-L1/PD-1 axis in MIA-induced offspring mice. Mechanistically, we found that MSC-EVs exerted a key role in glucose metabolism and neuroinflammation through PD-1/ERK/HIF-1α signaling in MIA offspring mice.

Abbreviations

2-DG	2-deoxy-D-glucose
ASD	Autism spectrum disorder
BCA	Bicinchoninic acid
CNS	Central nervous system
ELISA	Enzyme-linked immunosorbent assay
EPM	Elevated plus maze test
EVs	Extracellular versicles
GSEA	Gene set enrichment analysis
GO	Gene Ontology
HIF-1α	Hypoxia inducible factor 1
HK2	Hexokinase 2
IL	Interleukin
IFN-γ	Interferon-γ
KEGG	Kyoto Encyclopedia of Genes and Genomes
MBT	Marble burying test
MIA	Maternal immune activation
MSC	Mesenchymal stem cell
NOR	Novel object recognition test
OFT	Open field test
PD-1	Programmed death receptor 1
PD-L1	Programmed death ligand 1
PFC	Prefrontal cortex
LDHA	Lactate dehydrogenase A
Poly(I:C)	Polyinosinic polycytidylic acid
TEM	Transmission electron microscopy

Supplementary Information

The online version contains supplementary material available at https://doi.org/10.1186/s12951-025-03250-z.

Supplementary Material 1

Acknowledgements

We sincerely thank the assistance provided from Province Key Laboratory of Children development and genetic research (Harbin Medical University) and Key Laboratory of Preservation of Human Genetic Resources and Disease Control in China, Ministry of Education (Harbin Medical University).

Author contributions

QQ, SL and LJW conceptualized and designed experiments. QQ performed the animal and molecular experiments; data analysis; and wrote the original manuscript. QQ and LLF preprocessed and analyzed the molecular experiments. QQ, DYZ and YTJ performed primary microglia experiments. LLF, XZ and MYL performed bioinformatic analysis. HW (Han Wang), HW (Hui Wang), HL and SJL performed mice breeding and behavior experiments. SL obtained funding. SL and LJW critically reviewed the manuscript.

Funding
This study was supported by grants from the National Natural Science Foundation of China (81973068); the Excellent Young Teachers' Basic Research Support Program of Heilongjiang Province (YQJH2023040); the Open Project Program of Key Laboratory of Preservation of Human Genetic Resources and Disease Control in China (LPHGRDC2021-004).

Data availability
No datasets were generated or analysed during the current study.

Declarations

Ethics approval and consent to participate
The mouse experiments were approved by the Ethics Committee of Harbin Medical University (HMUIRB2023015).

Consent for publication
All authors agree with the publication of this paper.

Competing interests
The authors declare no competing interests.

Author details
[1]Department of Children's and Adolescent Health, Public Health College, Harbin Medical University, Harbin 150081, China

Received: 17 July 2024 / Accepted: 18 February 2025
Published online: 11 March 2025

References

1. Maenner MJ, Warren Z, Williams AR, Amoakohene E, Bakian AV, Bilder DA, Durkin MS, Fitzgerald RT, Furnier SM, Hughes MM, et al. Prevalence and characteristics of autism spectrum disorder among children aged 8 Years - autism and developmental disabilities monitoring network, 11 sites, united States, 2020. MMWR Surveill Summ. 2023;72:1–14.
2. Estes ML, McAllister AK. Maternal immune activation: implications for neuropsychiatric disorders. Science. 2016;353:772–7.
3. Kathuria A, Lopez-Lengowski K, Roffman JL, Karmacharya R. Distinct effects of interleukin-6 and interferon-gamma on differentiating human cortical neurons. Brain Behav Immun. 2022;103:97–108.
4. Careaga M, Taylor SL, Chang C, Chiang A, Ku KM, Berman RF, Van de Water JA, Bauman MD. Variability in polyic induced immune response: implications for preclinical maternal immune activation models. J Neuroimmunol. 2018;323:87–93.
5. Li X, Chauhan A, Sheikh AM, Patil S, Chauhan V, Li XM, Ji L, Brown T, Malik M. Elevated immune response in the brain of autistic patients. J Neuroimmunol. 2009;207:111–6.
6. Morgan JT, Chana G, Pardo CA, Achim C, Semendeferi K, Buckwalter J, Courchesne E, Everall IP. Microglial activation and increased microglial density observed in the dorsolateral prefrontal cortex in autism. Biol Psychiatry. 2010;68:368–76.
7. Hu Y, Mai W, Chen L, Cao K, Zhang B, Zhang Z, Liu Y, Lou H, Duan S, Gao Z. mTOR-mediated metabolic reprogramming shapes distinct microglia functions in response to lipopolysaccharide and ATP. Glia. 2020;68:1031–45.
8. Andersson AK, Rönnbäck L, Hansson E. Lactate induces tumour necrosis factor-alpha, interleukin-6 and interleukin-1beta release in microglial- and astroglial-enriched primary cultures. J Neurochem. 2005;93:1327–33.
9. Bardhan K, Anagnostou T, Boussiotis VA. The PD1:PD-L1/2 pathway from discovery to clinical implementation. Front Immunol. 2016;7:550.
10. Zhao J, Roberts A, Wang Z, Savage J, Ji RR. Emerging role of PD-1 in the central nervous system and brain diseases. Neurosci Bull. 2021;37:1188–202.
11. Ren X, Akiyoshi K, Vandenbark AA, Hurn PD, Offner H. Programmed death-1 pathway limits central nervous system inflammation and neurologic deficits in murine experimental stroke. Stroke. 2011;42:2578–83.
12. Guillot-Sestier MV, Doty KR, Gate D, Rodriguez J Jr., Leung BP, Rezai-Zadeh K, Town T. Il10 deficiency rebalances innate immunity to mitigate Alzheimer-like pathology. Neuron. 2015;85:534–48.
13. Gao X, Li W, Syed F, Yuan F, Li P, Yu Q. PD-L1 signaling in reactive astrocytes counteracts neuroinflammation and ameliorates neuronal damage after traumatic brain injury. J Neuroinflammation. 2022;19:43.
14. Siniscalco D, Giordano A, Galderisi U. Novel insights in basic and applied stem cell therapy. J Cell Physiol. 2012;227:2283–6.
15. Kawasaki Y, Sato K, Mashima K, Nakano H, Ikeda T, Umino K, Morita K, Izawa J, Takayama N, Hayakawa H, et al. Mesenchymal stromal cells inhibit aerobic Glycolysis in activated T cells by negatively regulating hexokinase II activity through PD-1/PD-L1 interaction. Transpl Cell Ther. 2021;27:231. e231-231 e238.
16. Li M, Soder R, Abhyankar S, Abdelhakim H, Braun MW, Trinidad CV, Pathak HB, Pessetto Z, Deighan C, Ganguly S, et al. WJMSC-derived small extracellular vesicle enhance T cell suppression through PD-L1. J Extracell Vesicles. 2021;10:e12067.
17. Yu X, Bai Y, Han B, Ju M, Tang T, Shen L, Li M, Yang L, Zhang Z, Hu G, et al. Extracellular vesicle-mediated delivery of circdym alleviates CUS-induced depressive-like behaviours. J Extracell Vesicles. 2022;11:e12185.
18. May T, Adesina I, McGillivray J, Rinehart NJ. Sex differences in neurodevelopmental disorders. Curr Opin Neurol. 2019;32:622–6.
19. Napolitano A, Schiavi S, La Rosa P, Rossi-Espagnet MC, Petrillo S, Bottino F, Tagliente E, Longo D, Lupi E, Casula L, et al. Sex differences in autism spectrum disorder: diagnostic, neurobiological, and behavioral features. Front Psychiatry. 2022;13:889636.
20. Haida O, Al Sagheer T, Balbous A, Francheteau M, Matas E, Soria F, Fernagut PO, Jaber M. Sex-dependent behavioral deficits and neuropathology in a maternal immune activation model of autism. Transl Psychiatry. 2019;9:124.
21. Arad M, Piontkewitz Y, Albelda N, Shaashua L, Weiner I. Immune activation in lactating dams alters sucklings' brain cytokines and produces non-overlapping behavioral deficits in adult female and male offspring: A novel neurodevelopmental model of sex-specific psychopathology. Brain Behav Immun. 2017;63:35–49.
22. Velmeshev D, Schirmer L, Jung D, Haeussler M, Perez Y, Mayer S, Bhaduri A, Goyal N, Rowitch DH, Kriegstein AR. Single-cell genomics identifies cell type-specific molecular changes in autism. Science. 2019;364:685–9.
23. Richetto J, Chesters R, Cattaneo A, Labouesse MA, Gutierrez AMC, Wood TC, Luoni A, Meyer U, Vernon A, Riva MA. Genome-Wide transcriptional profiling and structural magnetic resonance imaging in the maternal immune activation model of neurodevelopmental disorders. Cereb Cortex. 2017;27:3397–413.
24. Voineagu I, Wang X, Johnston P, Lowe JK, Tian Y, Horvath S, Mill J, Cantor RM, Blencowe BJ, Geschwind DH. Transcriptomic analysis of autistic brain reveals convergent molecular pathology. Nature. 2011;474:380–4.
25. Huang da W, Sherman BT, Lempicki RA. Systematic and integrative analysis of large gene lists using DAVID bioinformatics resources. Nat Protoc. 2009;4:44–57.
26. Subramanian A, Tamayo P, Mootha VK, Mukherjee S, Ebert BL, Gillette MA, Paulovich A, Pomeroy SL, Golub TR, Lander ES, Mesirov JP. Gene set enrichment analysis: a knowledge-based approach for interpreting genome-wide expression profiles. Proc Natl Acad Sci U S A. 2005;102:15545–50.
27. Cheng YY, Chen BY, Bian GL, Ding YX, Chen LW. Programmed Death-1 deficiency aggravates motor dysfunction in MPTP model of Parkinson's disease by inducing microglial activation and neuroinflammation in mice. Mol Neurobiol. 2022;59:2642–55.
28. t Hart BA, den Dunnen WF. Commentary on special issue: CNS diseases and the immune system. J Neuroimmune Pharmacol. 2013;8:757–9.
29. Lammert CR, Lukens JR. Modeling Autism-Related disorders in mice with maternal immune activation (MIA). Methods Mol Biol. 2019;1960:227–36.
30. Larochelle C, Alvarez JI, Prat A. How do immune cells overcome the blood-brain barrier in multiple sclerosis? FEBS Lett. 2011;585:3770–80.
31. Krstic D, Madhusudan A, Doehner J, Vogel P, Notter T, Imhof C, Manalastas A, Hilfiker M, Pfister S, Schwerdel C, et al. Systemic immune challenges trigger and drive Alzheimer-like neuropathology in mice. J Neuroinflammation. 2012;9:151.
32. Edmonson C, Ziats MN, Rennert OM. Altered glial marker expression in autistic post-mortem prefrontal cortex and cerebellum. Mol Autism. 2014;5:3.
33. Suzuki K, Sugihara G, Ouchi Y, Nakamura K, Futatsubashi M, Takebayashi K, Yoshihara Y, Omata K, Matsumoto K, Tsuchiya KJ, et al. Microglial activation in young adults with autism spectrum disorder. JAMA Psychiatry. 2013;70:49–58.
34. Masi A, Glozier N, Dale R, Guastella AJ. The immune system, cytokines, and biomarkers in autism spectrum disorder. Neurosci Bull. 2017;33:194–204.

35. Onore CE, Schwartzer JJ, Careaga M, Berman RF, Ashwood P. Maternal immune activation leads to activated inflammatory macrophages in offspring. Brain Behav Immun. 2014;38:220–6.
36. Weissman JR, Kelley RI, Bauman ML, Cohen BH, Murray KF, Mitchell RL, Kern RL, Natowicz MR. Mitochondrial disease in autism spectrum disorder patients: a cohort analysis. PLoS ONE. 2008;3:e3815.
37. El Fotoh W, El Naby SAA, Abd El Hady NMS. Autism spectrum disorders: the association with inherited metabolic disorders and some trace elements. A retrospective study. CNS Neurol Disord Drug Targets. 2019;18:413–20.
38. Khemakhem AM, Frye RE, El-Ansary A, Al-Ayadhi L, Bacha AB. Novel biomarkers of metabolic dysfunction is autism spectrum disorder: potential for biological diagnostic markers. Metab Brain Dis. 2017;32:1983–97.
39. Correia C, Coutinho AM, Diogo L, Grazina M, Marques C, Miguel T, Ataide A, Almeida J, Borges L, Oliveira C, et al. Brief report: high frequency of biochemical markers for mitochondrial dysfunction in autism: no association with the mitochondrial aspartate/glutamate carrier SLC25A12 gene. J Autism Dev Disord. 2006;36:1137–40.
40. Hagihara H, Catts VS, Katayama Y, Shoji H, Takagi T, Huang FL, Nakao A, Mori Y, Huang KP, Ishii S, et al. Decreased brain pH as a shared endophenotype of psychiatric disorders. Neuropsychopharmacology. 2018;43:459–68.
41. Licznerski P, Park HA, Rolyan H, Chen R, Mnatsakanyan N, Miranda P, Graham M, Wu J, Cruz-Reyes N, Mehta N, et al. ATP synthase c-Subunit leak causes aberrant cellular metabolism in fragile X syndrome. Cell. 2020;182:1170–e11851179.
42. Wang M, Xian P, Zheng W, Li Z, Chen A, Xiao H, Xu C, Wang F, Mao H, Meng H, et al. Axin2 coupled excessive Wnt-glycolysis signaling mediates social defect in autism spectrum disorders. EMBO Mol Med. 2023;15:e17101.
43. Vallee A, Vallee JN. Warburg effect hypothesis in autism spectrum disorders. Mol Brain. 2018;11:1.
44. Cheng J, Zhang R, Xu Z, Ke Y, Sun R, Yang H, Zhang X, Zhen X, Zheng LT. Early glycolytic reprogramming controls microglial inflammatory activation. J Neuroinflammation. 2021;18:129.
45. Xin WQ, Wei W, Pan YL, Cui BL, Yang XY, Bahr M, Doeppner TR. Modulating poststroke inflammatory mechanisms: novel aspects of mesenchymal stem cells, extracellular vesicles and microglia. World J Stem Cells. 2021;13:1030–48.
46. Cone AS, Yuan X, Sun L, Duke LC, Vreones MP, Carrier AN, Kenyon SM, Carver SR, Benthem SD, Stimmell AC, et al. Mesenchymal stem cell-derived extracellular vesicles ameliorate Alzheimer's disease-like phenotypes in a preclinical mouse model. Theranostics. 2021;11:8129–42.
47. Zhang Y, Ma CJ, Ni L, Zhang CL, Wu XY, Kumaraguru U, Li CF, Moorman JP, Yao ZQ. Cross-talk between programmed death-1 and suppressor of cytokine signaling-1 in Inhibition of IL-12 production by monocytes/macrophages in hepatitis C virus infection. J Immunol. 2011;186:3093–103.
48. Zhuang ZY, Gerner P, Woolf CJ, Ji RR. ERK is sequentially activated in neurons, microglia, and astrocytes by spinal nerve ligation and contributes to mechanical allodynia in this neuropathic pain model. Pain. 2005;114:149–59.
49. Lu H, Lin J, Xu C, Sun M, Zuo K, Zhang X, Li M, Huang H, Li Z, Wu W, et al. Cyclosporine modulates neutrophil functions via the SIRT6-HIF-1alpha-glycolysis axis to alleviate severe ulcerative colitis. Clin Transl Med. 2021;11:e334.
50. Pan T, Sun S, Chen Y, Tian R, Chen E, Tan R, Wang X, Liu Z, Liu J, Qu H. Immune effects of PI3K/Akt/HIF-1alpha-regulated Glycolysis in polymorphonuclear neutrophils during sepsis. Crit Care. 2022;26:29.
51. Obaidi I, Blanco Fernandez A, McMorrow T. Curcumin Sensitises Cancerous Kidney Cells to TRAIL Induced Apoptosis via Let-7 C Mediated Deregulation of Cell Cycle Proteins and Cellular Metabolism. Int J Mol Sci. 2022;23:9569.
52. Zhang ZG, Buller B, Chopp M. Exosomes - beyond stem cells for restorative therapy in stroke and neurological injury. Nat Rev Neurol. 2019;15:193–203.
53. Xin H, Li Y, Cui Y, Yang JJ, Zhang ZG, Chopp M. Systemic administration of exosomes released from mesenchymal stromal cells promote functional recovery and neurovascular plasticity after stroke in rats. J Cereb Blood Flow Metab. 2013;33:1711–5.
54. Zhao J, Bang S, Furutani K, McGinnis A, Jiang C, Roberts A, Donnelly CR, He Q, James ML, Berger M, et al. PD-L1/PD-1 checkpoint pathway regulates hippocampal neuronal excitability and learning and memory behavior. Neuron. 2023;111:2709–e27262709.

Publisher's note